Article

Cell Host & Microbe

Human neutralizing antibodies targeting the measles virus hemagglutinin and fusion surface proteins

Graphical abstract

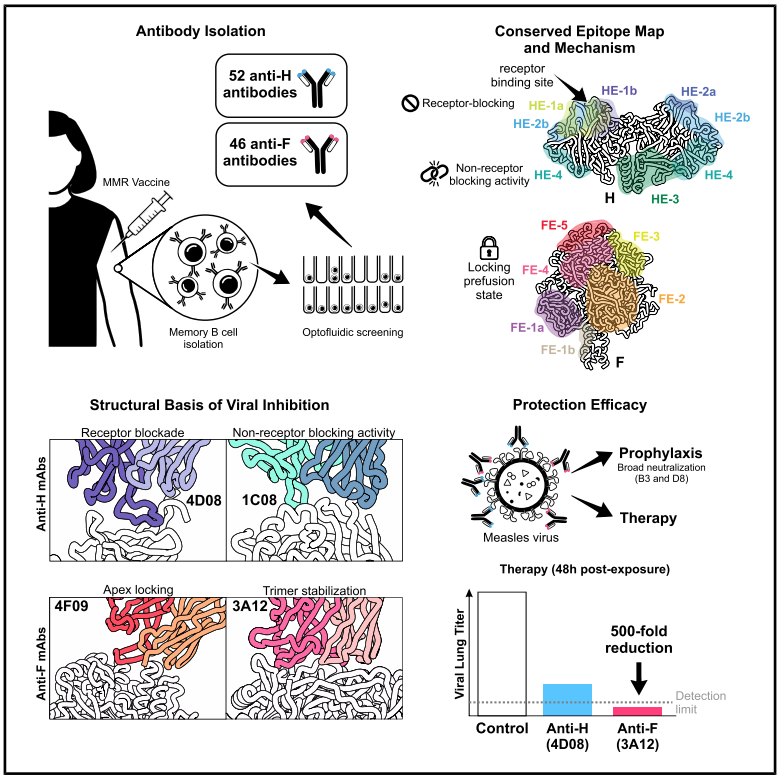

Highlights

- Measles-specific mAbs were isolated from a human MMR vaccinee, years after vaccination
- MAbs recognize four major sites on hemagglutinin (H) and five on the fusion (F) protein
- Lead mAbs against H and F exhibit picomolar neutralization via diverse mechanisms
- Anti-H and -F mAbs reduce viral loads *in vivo*, even when given 48 h after infection

Authors

Marissa Acciani, Dawid Zyla, Gele Niemeyer, ..., Matteo Porotto, Kathryn M. Hastie, Erica Ollmann Saphire

Correspondence

kmhastie@lji.org (K.M.H.), erica@lji.org (E.O.S.)

In brief

Acciani, Zyla et al. identify a panel of human monoclonal antibodies against measles virus surface proteins. These antibodies neutralize with picomolar potency, target conserved sites, broadly neutralize diverse strains, and protect animals even after exposure, highlighting opportunities to prevent or treat measles as outbreaks re-emerge.

Acciani et al., 2026, Cell Host & Microbe *34*, 1–15
June 10, 2026
https://doi.org/10.1016/j.chom.2026.04.010

CellPress

Cell Host & Microbe

CellPress
OPEN ACCESS

Article

Human neutralizing antibodies targeting the measles virus hemagglutinin and fusion surface proteins

Marissa Acciani,[1,9] Dawid Zyla,[1,9] Gele Niemeyer,[1,2] Stephanie Harkins,[1] Diptiben Parekh,[1] Emily Pawlack,[3] Davide Lacarbonara,[4] Dhvanir Kansara,[5] Margaret E. Ackerman,[6] Stefan Niewiesk,[3] Matteo Porotto,[4,7,8] Kathryn M. Hastie,[1,*] and Erica Ollmann Saphire[1,2,10,*]

[1]Center for Vaccine Innovation, La Jolla Institute for Immunology, La Jolla, CA 92037, USA
[2]School of Medicine, University of California, San Diego, La Jolla, CA 92093, USA
[3]Department of Veterinary Biosciences, College of Veterinary Medicine, The Ohio State University, Columbus, OH 43210, USA
[4]Department of Pediatrics, Columbia University Vagelos College of Physicians and Surgeons, New York, NY 10032, USA
[5]Department of Microbiology and Immunology, Geisel School of Medicine, Dartmouth College, Hanover, NH 03755, USA
[6]Thayer School of Engineering, Dartmouth College, Hanover, NH 03755, USA
[7]Center for Host-Pathogen Interaction, Columbia University Vagelos College of Physicians and Surgeons, New York, NY 43210, USA
[8]Department of Woman, Child and General and Specialized Surgery, University of Campania Luigi Vanvitelli, 81100 Caserta, Italy
[9]These authors contributed equally
[10]Lead contact
*Correspondence: kmhastie@lji.org (K.M.H.), erica@lji.org (E.O.S.)
https://doi.org/10.1016/j.chom.2026.04.010

SUMMARY

Measles virus (MeV), a highly transmissible paramyxovirus, can cause severe complications and death, particularly in infants and young children. How and where human antibodies target and neutralize MeV remain unclear. Here, we report a panel of human monoclonal antibodies (mAbs) specific for MeV hemagglutinin (H) and fusion (F) surface proteins, derived from the memory B cells of a Measles-Mumps-Rubella (MMR) vaccinee. We mapped four and five major epitope clusters on H and F, respectively, and structurally characterized representative mAbs from each epitope cluster. MAbs against both H and F offer broad, potent, picomolar-level neutralization and substantially reduce viral loads *in vivo* when delivered before or after viral exposure. High-resolution cryo-electron microscopy of mAb complexes with H and F reveal highly conserved contact sites of the most protective antibodies. Characterization of these fully human mAbs provides avenues for prophylactic or therapeutic intervention against re-emerging MeV.

INTRODUCTION

Measles virus (MeV), an enveloped negative-sense RNA paramyxovirus, is one of the most highly transmissible viruses known, with an estimated basic reproductive number (R_0) of 12–18.[1] MeV infection causes symptoms including fatal respiratory and neurological complications,[2] and increases risk of secondary infections due to "immune amnesia," an immunosuppressive state lasting weeks to years after acute infection.[3,4]

A live-attenuated vaccine derived from a genotype A MeV strain provides vaccinees with lifelong immunity and protective antibodies against all 24 MeV genotypes in circulation.[5] Despite the global presence of MeV and widespread use of the vaccine, few studies have mapped the human antibody response. We do not yet know how human antibodies, from either measles vaccination or natural infection, recognize and protect against the virus.

Protective antibodies against MeV may target one of two essential surface glycoproteins, hemagglutinin (H) and fusion (F), which together mediate virus-cell entry. MeV H is a single-pass transmembrane protein that forms dimers or loosely assembled tetramers[6–9] on the viral surface and binds cellular receptors signaling lymphocyte activating molecule family member 1 (SLAMF1 or CD150) on alveolar macrophages, dendritic cells, and lymphocytes and nectin-4 on respiratory epithelial cells. Laboratory-adapted MeV H may also use CD46 as a receptor.[10]

MeV F is a metastable class I trimer composed of disulfide-linked F1 and F2 subunits. Upon H-receptor engagement, F undergoes structural rearrangements that drive membrane fusion. The F1 heptad repeats refolding to project the fusion peptide into the host membrane via an extended prehairpin intermediate, followed by collapse into a stable six-helix bundle to create the fusion pore.[11]

Human vaccinees generate antibodies against both MeV H and F, and protection against measles infection correlates best with the level of neutralizing antibodies targeting H.[12–19] Interestingly, neutralizing anti-F antibodies have thus far been reported only in individuals infected with wild-type virus.[16]

Please cite this article in press as: Acciani et al., Human neutralizing antibodies targeting the measles virus hemagglutinin and fusion surface proteins, Cell Host & Microbe (2026), https://doi.org/10.1016/j.chom.2026.04.010

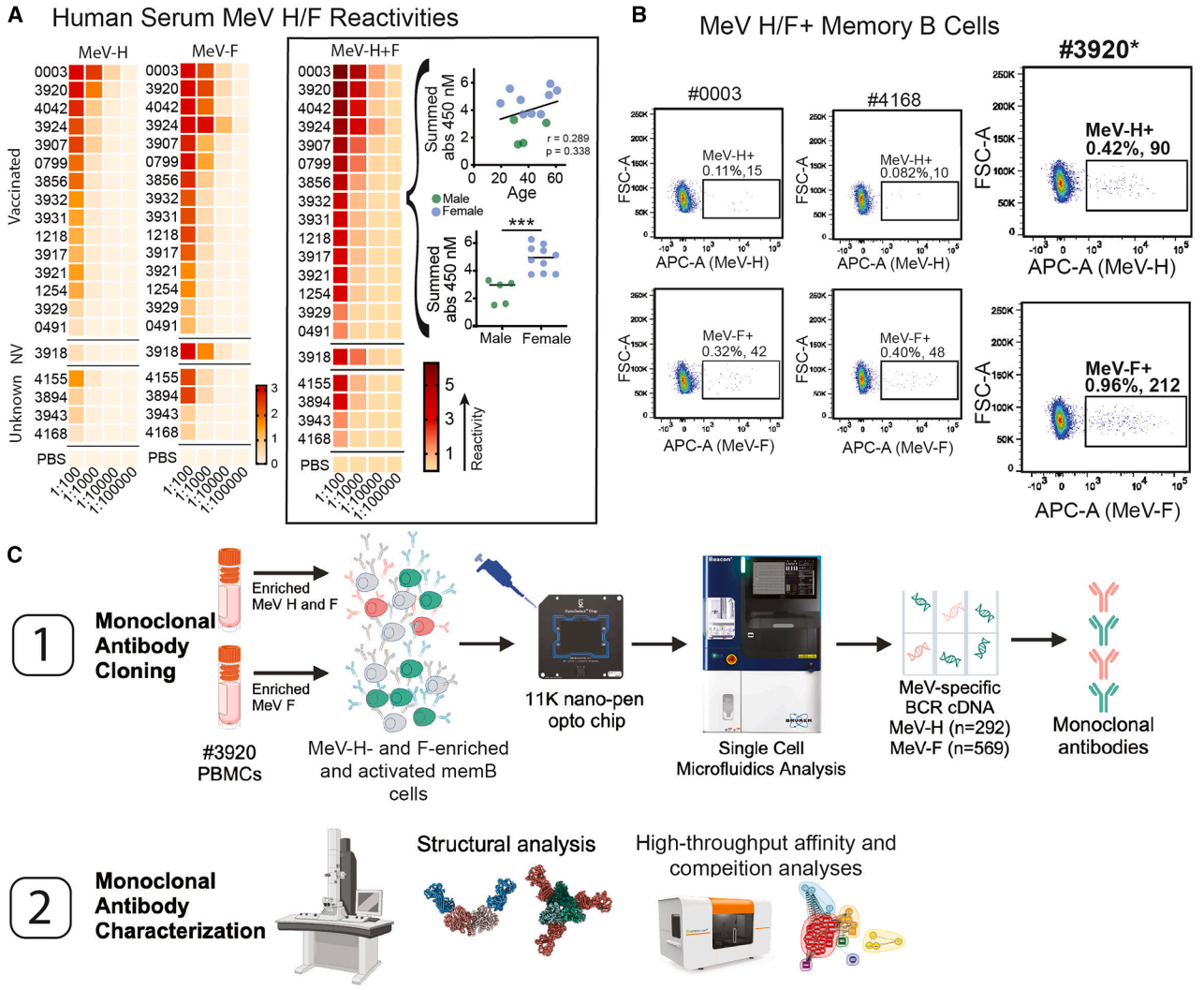

Figure 1. Vaccinee donor selection and MeV-specific memory B cell isolation

(A) Sera from 20 individuals were screened for polyclonal antibody recognition of MeV H_{FL} or F_{FL} via ELISA ("NV" = not vaccinated). Reactivities for each individual were quantified by measuring optical density (OD) at 450 nm, with data displayed in a heatmap (red = higher reactivity, beige = lower reactivity). Reactivities were summed across antigens (right outline). Summed sera reactivities (diluted 1:100) of vaccinated donors are also plotted by age and sex (females shown in blue, [n = 10]; males shown in green [n = 5]), ***$p < 0.0005$ by unpaired t test.

(B) PBMCs from three vaccinees were surface-stained and single, live, MeV H+ or F+ memory B cells were quantified using flow cytometry.

(C) PBMCs from vaccinee #3920 were enriched for MeV H or F, activated into mAb-secreting cells, and loaded into a Beacon (Bruker) for high-throughput single cell analysis.

See also Figure S1.

Mapping of MeV immune recognition has relied primarily on murine monoclonal antibodies (mAbs) and a combination of functional assays, mutagenesis, and peptide-based approaches.[17,20–29] The relevance of several of these sites to humans has been evaluated using polyclonal human sera.[17,20,23,24,30–32] However, to date, no structures of H or F bound to any human antibody have been reported.

Here, we sought to map the human antibody response against MeV. We isolated mAbs from the peripheral memory B cells of a vaccinated 56-year-old female, resolved structures of mAb-H/F complexes, mapped the epitopes associated with each competition group, and evaluated antibody functions *in vitro* and *in vivo*.

RESULTS

Isolation of antibodies from a thrice-vaccinated person

We screened sera from a human donor pool (n = 20) in La Jolla, California for polyclonal antibody reactivity to reference strains of full-length MeV H and full-length prefusion-stabilized F[33,34] glycoproteins to select a candidate for mAb discovery (Figure 1). We sorted individuals by vaccination status and summed H/F sera reactivities (Figure 1A, outlined). Correlative analyses of summed reactivity versus age and sex for this relatively small vaccinated donor pool showed that female donors (n = 10) had significantly higher reactivity to measles antigens than male

Please cite this article in press as: Acciani et al., Human neutralizing antibodies targeting the measles virus hemagglutinin and fusion surface proteins, Cell Host & Microbe (2026), https://doi.org/10.1016/j.chom.2026.04.010

CellPress
OPEN ACCESS

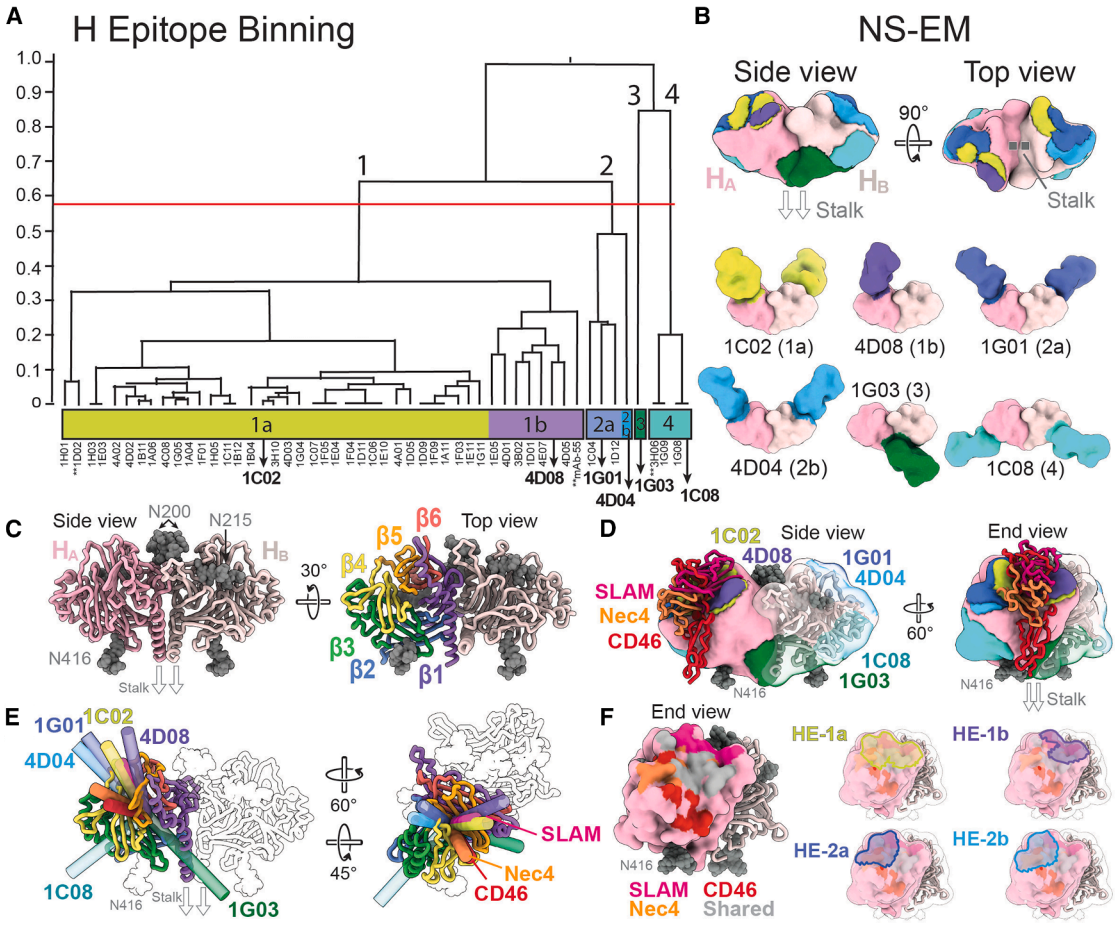

Figure 2. MAb epitope mapping on MeV H_{ECT}

(A) High-throughput competition assays of mAbs with H_{ECT} were performed using a Carterra Lodestar Array (LSA). Murine mAb55 was included as a control.[20,37] MAbs were assigned to epitope groups, as represented by a binning dendrogram. Coarser epitope communities were generated by manually adjusting the dendrogram cut-height (red line). MAbs selected for NS-EM are bolded. Starred mAbs (**) were not directly visualized but were included in *in vitro* experiments.

(B) Fab-H_{ECT} complexes were subjected to NS-EM. Alphafold-derived structural models for H_{ECT} and murine Fab55 were docked into NS-EM densities, and Fab binding footprints were mapped onto H_{ECT} molecular surfaces.

(C) H_{ECT} dimer modeled with homogeneous N-linked glycans[8,38] ($GlcNAc_2Man_5$, gray spheres) and individual B propeller blades annotated.

(D) H_{ECT}-Fab footprint mapping combined with known H-SLAMF1 (PDB: 3ALZ), -nectin-4 (PDB: 4GJT), and -CD46 (PDB: 3INB) structures.

(E) MAb and receptor approach angles relative to H_{ECT} were visually inspected by defining molecular axes.

(F) Surface-exposed receptor contact residues on H are shown in the indicated colors, with mAb epitopes overlaid on the H molecular surface for direct comparison. All structures were illustrated using Chimera X.[83]

See also Figures S2, S3, and S7; Tables S1 and S4; and Data S1.

donors (n = 5). Using flow cytometry, we also observed an ~3-fold higher incidence of F-specific memory B cells relative to H-specific B cells in a subset of three donors (Figure 1B).

For mAb discovery, we selected donor #3920 (Figure 1C), a 56-year-old individual who reported receiving two MeV vaccine doses in childhood and a third dose as an adult, 5 years before sample donation. This donor's peripheral blood mononuclear cells (PBMCs) were enriched for MeV-specific memory B cells using biotinylated ectodomain (H_{ECT} and F_{ECT}) probes. Activated MeV H- and F-specific memory B cells were loaded onto a Bruker Cell Analysis Beacon for individual cell selection. Heavy- and light-chain-variable regions from 384 H- and F-specific cells were sequenced, cloned, and expressed as individual mAbs in ExpiCHO cells (Figure S1A). We observed an inverse correlation between affinity and virus inhibition for F-specific mAbs, and no link between affinity/inhibition and heavy-chain-variable germline usage for H- and F-specific mAbs (Figure S1B).

Defining human mAb epitopes on H and F

Anti-H (n = 52) and anti-F mAbs (n = 46) were purified and assessed for antigen-binding kinetics and competition behaviors, then sorted into four and five epitope communities, respectively (Figures 2A and 3A; Table S1). Representative mAbs from each community were selected for direct footprint mapping using negative-stain electron microscopy (NS-EM). High-quality micrographs of antigen-Fab complexes were used to construct

Please cite this article in press as: Acciani et al., Human neutralizing antibodies targeting the measles virus hemagglutinin and fusion surface proteins, Cell Host & Microbe (2026), https://doi.org/10.1016/j.chom.2026.04.010

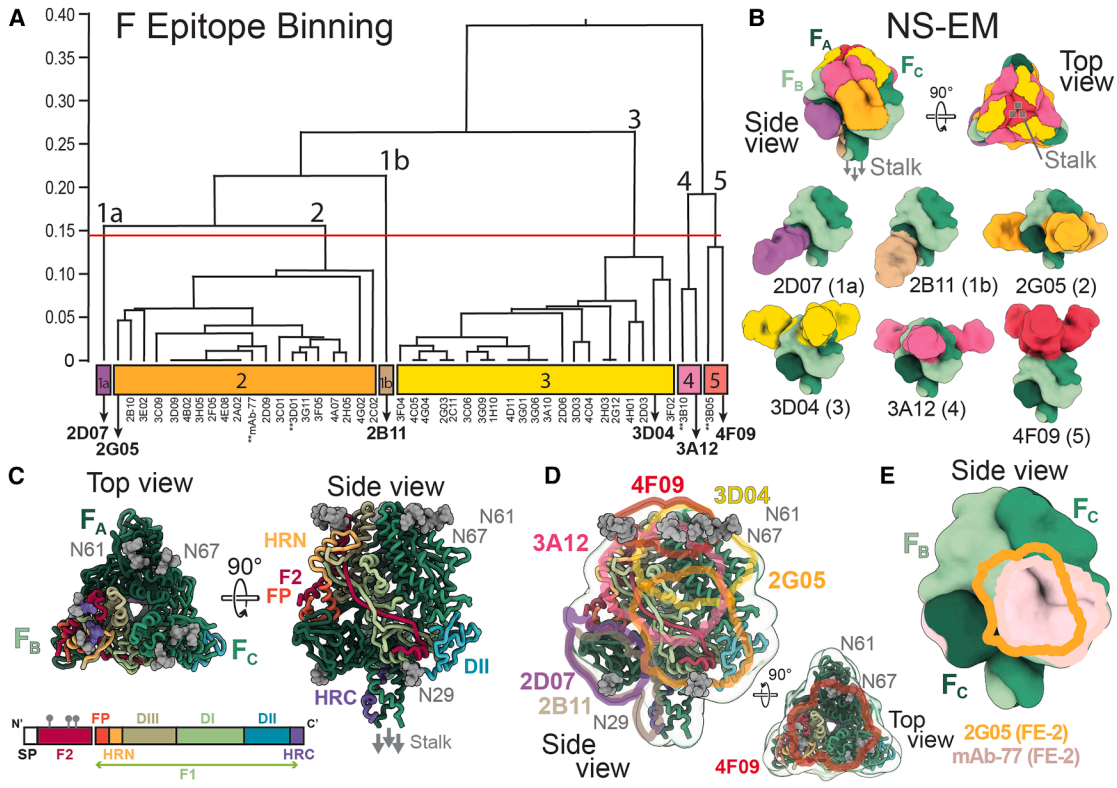

Figure 3. MAb epitope mapping on MeV F

(A) High-throughput competition assays of purified mAbs with F_{ECT} were performed using a Carterra LSA. Murine mAb-77[34] was also included. MAbs were assigned to epitope groups, as represented by a binning dendrogram. Coarser epitope communities were generated by manually adjusting the dendrogram cut height (red line). MAbs selected for NS-EM are bolded; starred mAbs (**) were not directly visualized but were included in *in vitro* experiments.

(B) Fab-antigen complexes were subjected to NS-EM. The cryo-EM-derived structural model for F_{ECT} (PDB: 8UT2) and a Fab alphafold model were docked into NS-EM densities, and Fab binding footprints were mapped onto F_{ECT} molecular surfaces.

(C) The F_{ECT} trimer modeled with N-linked glycans (gray spheres), with functional and structural domains annotated for one protomer; SP, signal peptide; FP, fusion peptide; HRN, N-terminal heptad repeat; DI-III, domains I-III; and HRC, C-terminal heptad repeat.

(D) F-Fab footprint mapping overlaid on the annotated F_{ECT} trimer, accompanied by a smaller apex view to better visualize epitope FE-5.

(E) Footprints for FE-2 mAbs 2G05 and mAb-77 overlaid on the F_{ECT} trimer. All structures were illustrated using Chimera X.[39]

See also Figures S2, S3, and S7; Table S1; and Data S2.

3D densities in cryoSPARC.[35] Individual H_{ECT} and F_{ECT} models and Fabs were docked into densities in ChimeraX[36] (Figures 2B, 3B, and S2; Data S1 and S2).

For H-Fab complexes, we used a previously characterized purified H_{ECT}, which forms disulfide-linked dimers of globular head domains.[8] Each head domain contains a six-bladed beta propeller (four antiparallel β-strands per blade) with N-linked glycans at N200, N215, and N416 (Figure 2C).[8,38] We term the four major H epitope communities HE-1 through HE-4. HE-1 and -2 contain sub-communities designated HE-1a and HE-1b, and HE-2a and HE-2b, on the apical surface of the dimer (Figures 2A and 2B). Most (42/52, or 81%) purified mAbs are HE-1, suggesting it could be a major immunogenic site. HE-1 overlaps with binding sites for MeV receptors SLAMF1, nectin-4, and CD46 (Figures 2D–2F).[7,9,38] HE-1a encompasses the inside and outer edges of a concave groove formed by H propeller blades β4, β5, and β6, which also contains the binding sites for SLAMF1[7] and nectin-4.[38] HE-1b covers a smaller region shifted toward the anterior edge of the groove, which is closer to blades β5 and β6 (Figure 2F). MAbs 1C02 (HE-1a) and 4D08 (HE-1b) approach the groove at almost an identical angle relative to SLAMF1 (Figure 2E).

HE-2 maps to the posterior edge of this groove to a region containing blades β3, β4, and β5 and extends toward the dimer's posterior face. HE-2a, defined by mAb 1G01, localizes more apically at the flexible loop connecting blades β4 and β5, while HE-2b, defined by mAb 4D04, spans an area encompassing blades β3 and β4 at the dimer's periphery.

HE-3 and HE-4, defined by mAbs 1G03 and 1C08, respectively, approach the membrane-proximal undersides of the globular head domains where mAb 1G03 (HE-3), which binds one Fab per dimer, recognizes the dimer interface to engage the β1 blade of both monomers and blades β1–β3 of a single monomer. This epitope may be vulnerable to glycan shielding by the N-linked glycan at N416. HE-4 mAb 1C08 binds two Fabs per dimer and symmetrically recognizes the peripheral ends of each monomer at blades β2 and β3. Overall, the majority of the exposed H dimer surface was targeted by mAbs, with

Please cite this article in press as: Acciani et al., Human neutralizing antibodies targeting the measles virus hemagglutinin and fusion surface proteins, Cell Host & Microbe (2026), https://doi.org/10.1016/j.chom.2026.04.010

a high incidence of mAbs targeting the receptor-binding regions.

We next complexed F-reactive Fabs to purified F_{ECT} trimers, which lack the transmembrane domain and cytoplasmic tail and contain naturally occurring mutations that slow the post-fusion transition.[34] The F1 and F2 subunits contain N-linked glycans at positions N61 and N67 at the trimer apex and N29 at the membrane-proximal undersides of each monomer. Five major antibody recognition sites ascend the prefusion F trimer vertically and are evenly distributed across the base to the apex to nearly cover the entire trimer surface (Figure 3B). FE-1, defined by mAbs 2D07 (FE-1a) and 2B11 (FE-1b), localizes to the F1 subunit domain II at the trimer base corners. These mAbs were sorted into individual, separate epitope communities and did not fully saturate all epitopes on the F trimer, as observed in NS-EM 2D classes.

Most F-specific mAbs are grouped into FE-2 (19/46, 41%) and FE-3 (21/46, 46%), which map to the trimer's lower and upper faces, respectively. FE-2 mAbs target the N' α-helix and a large surface-exposed β strand in the F2 subunit (approximately residues 1–45) that stretches from the bottom right to upper left face of each monomer in the trimer, as well as a portion of domain II (DII). Murine mAb-77[26,34,40] is also FE-2, and its footprint is highly similar to that of human mAb 2G05 (Figure 3E).[34] FE-3 approaches the upper right edge of the trimer face, targeting an epitope that encompasses the C' F2 α helix and F1 N-terminal heptad repeat (HRN).

FE-4 is located centrally on the trimer face, vertically positioned between epitopes FE-2 and FE-3. This epitope includes more membrane-distal regions of the N' F2 β strand and may include the C' F2 α helix. FE-5 is at the trimer apex and contains loops or hinge regions between secondary structures in the HRN, F2, and DIII domains. FE-5 contains only 4F09 and 3B05, and this low frequency may be due to glycan shielding at N61 and N67.

We identified a correlation between epitope specificity and mAb germline gene usage for F-specific mAbs. FE-1 and FE-2 mAbs, which target the trimer base, predominantly use immunoglobulin heavy chain variable 3 (IGHV3) family genes, whereas FE-3, FE-4, and FE-5 mAbs are derived from IGHV1 and IGHV4 family genes (Table S1).

We evaluated the ability of AlphaFold3 (AF3) multimer modeling to predict mAb binding sites to within NS-EM accuracy and found that it successfully predicted sites for only a small fraction (2/12) of the visualized complexes, reinforcing the need for experimental determination of epitopes (Figure S3).

MeV mAb *in vitro* and prophylactic *in vivo* efficacy

We next measured *in vitro* neutralization potency of the mAbs against a recombinant MeV-B3 strain (rMeV-B3-mCherry), corresponding to a currently circulating wild-type virus (Figure 4A).[5]

Mabs targeting HE-1a, HE-1b, HE-2a, and HE-2b near the receptor-binding site are highly neutralizing (IC_{50} [half-maximal inhibitory concentration] 0.01–1.174 nM; Figure 4B, left; Table S1). HE-3 mAb, 1G03, targeting the H dimer interface, does not neutralize. HE-4 mAbs, which bind at the H periphery, have variable potency with mAb 1C08, a top neutralizer in the panel (IC_{50} 0.071 nM), and 3H06, which is non-neutralizing.

Anti-F mAbs in FE-3, FE-4, and FE-5 also potently neutralize with IC_{50}s ranging from 0.192 to 0.733 nM (Figure 4B, right). FE-2 mAbs 2G05 and mAb-77[34] neutralize with IC_{50}s 1.577 and 0.333 nM, respectively, while FE-2 mAb 3D01 does not neutralize. FE-1 mAbs 2D07 and 2B11 neutralize poorly with IC_{50} values of 22.29 and 432.3 nM, respectively (Table S1).

Overall, F-specific mAbs binding the top half of the trimer demonstrate more potent neutralization than those against the bottom half of the trimer. The most potent neutralizing F mAbs, 3B10 and 3B05 (IC_{50}s 0.192 and 0.21 nM, respectively), target epitopes FE-4 and FE-5, which are both quaternary epitopes at the upper face and apex of F, respectively.

We next assessed the protective activities of these human mAbs in the cotton rat model, a semi-permissive animal model that replicates key aspects of human MeV infection, including wild-type viral replication in the lungs via H-SLAMF1 interactions.[41,42] Cotton rats were pre-treated with mAbs then infected with rMeV-B3-eGFP.[34] Lung tissues were harvested at peak infection, and MeV titers were quantified (Figures 4C and S4A). Two mAbs against H (4D08, HE-1b, receptor-binding site; 1C08, HE-4, periphery) and four mAbs against F (3B10, FE-4, upper center; 3D04, FE-3, lower right; 3A12, FE-4, upper center; and 4F09, FE-5, apex) are highly protective, reducing MeV lung titers ∼50–200-fold. The anti-F apex-binding mAb 4F09 is the most protective, reducing lung titers to undetectable levels.

In vitro neutralization potency generally correlates with *in vivo* prophylactic protection ($r = 0.4964$, $p = 0.0623$) for neutralizing mAbs. Several neutralizing mAbs (2G05 [F], 1C02 [H], and 1G01 [H]) require a five-fold higher dose (5 mg/kg) to demonstrate protective efficacy in this model (Figure S4B).

We probed the abilities of H-specific mAbs to block receptor binding using soluble human SLAMF1 fused to human Fc (Fig 4C), and we found that HE-1a (1C02 and 1D02) and -1b (4D08 and murine mAb55) mAbs directly compete with this immune cell receptor. Blocking receptor binding is therefore a likely mechanism of neutralization by these mAbs. We previously characterized murine mAbs against MeV F that neutralize by stabilizing or destabilizing the prefusion F trimer.[43] We examined whether our human anti-F mAbs demonstrate these functionalities by measuring F thermal stability alone and in complex with mAbs using nanoscale differential scanning fluorimetry (nanoDSF) (Figure 4D). FE-3, -4, and -5 mAbs, targeting the upper trimer face and apex, increase the melting temperature of the F trimer 5.9°C to 23°C, respectively. Notably, mAbs 4F09 (FE-5) and 3A12 (FE-4) shift the melting temperature 19°C and 23°C, respectively, the highest trimer-stabilizing effects recorded for any F-specific mAb. Considering these mAbs are the most potent neutralizers and prophylactic protectors among our panel (Figures 4A and 4B), we can conclude that F prefusion trimer stabilization is a major mechanism of MeV inhibition through F.

We also evaluated mAb Fc effector functionality, including antibody-dependent cellular phagocytosis (ADCP, Figure S4C), cellular cytotoxicity (ADCC, Figure S4D), and complement deposition (ADCD, Figure S4E). Among H-specific mAbs, Fc-mediated activities may contribute to protection. The two most protective mAbs exhibit either high levels of all three functions (1C08) or high levels of just ADCD (4D08). mAb 1C02, which neutralizes *in vitro* but does not protect *in vivo*, does not exhibit high levels of ADCD.

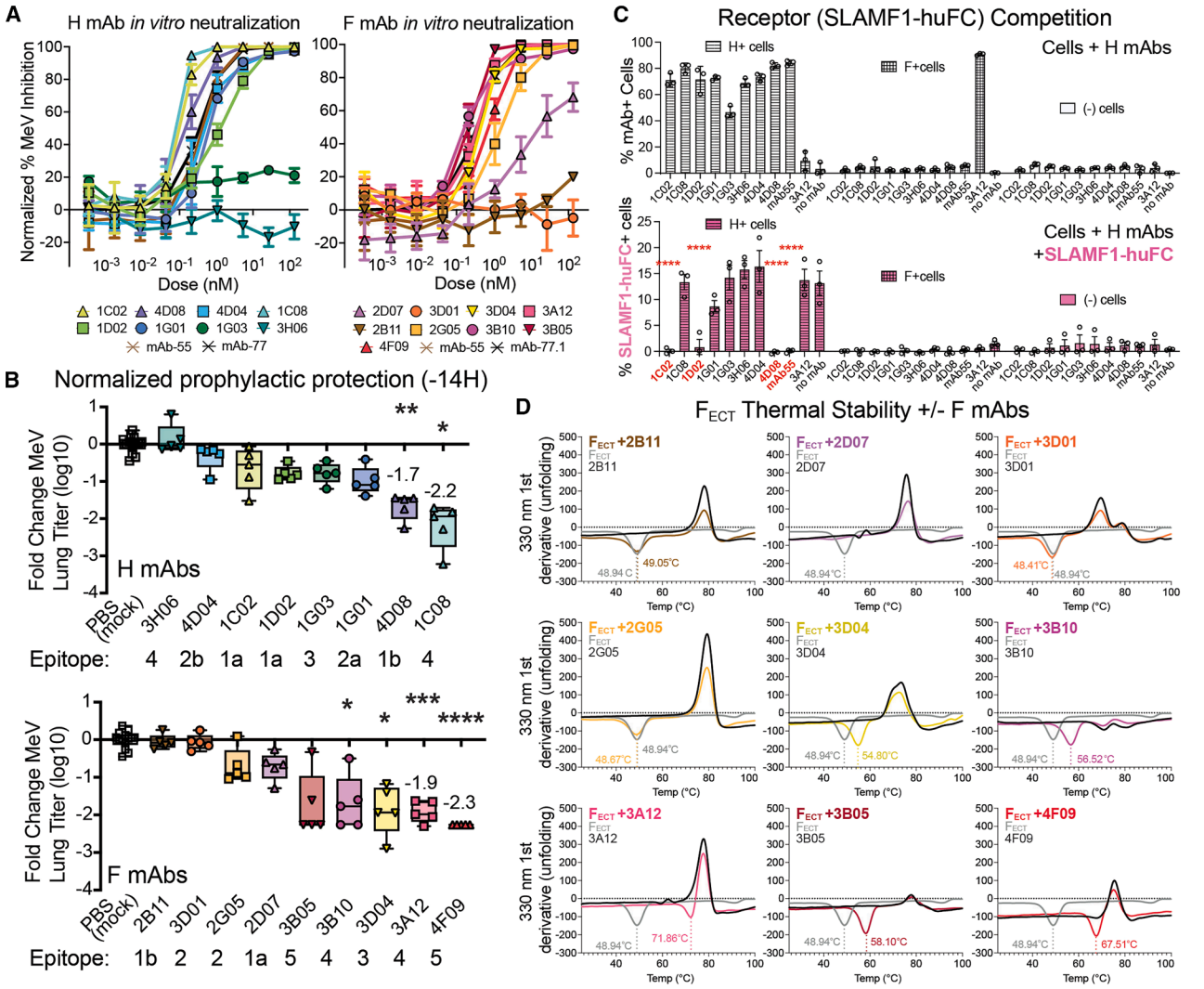

Figure 4. MeV mAb *in vitro* and prophylactic *in vivo* efficacy

(A) MAbs were combined with rMeV-B3 (5×10^3 PFU/mL) and applied to vero-SLAMF1 cells to assess neutralization efficiencies. Neutralizing murine mAbs 55[37] and 77[34] were included as controls. The next day, mCherry-infected cells were quantified using a CellInsight CX5 plate reader (ThermoFisher). Data were normalized to percentage MeV inhibition using untreated infected wells, average ± SEM (n = 3–4 biological replicates).

(B) MeV titer reduction in cotton rat lungs ($TCID_{50}$log10/g lung tissue, or the log-transformed half-maximal tissue culture infectious dose per gram lung tissue), normalized and displayed as fold-change compared with intra-group PBS controls. Cotton rats were injected with mAbs (1 mg/kg, 5 animals per mAb), or PBS (3–4 animals) 14 h before infection. Animals were then inoculated with 2×10^5 $TCID_{50}$ rMeV-B3-GFP. 4 days after infection, lung tissue homogenates were prepared, serially diluted, and titrated on vero-SLAMF1 cells. Average PBS-treated lung titers ($TCID_{50}$log10/g lung tissue) were subtracted from mAb-treated lung titers, and the average reduction of lung titers (fold-change MeV lung titer log10) for each mAb treatment are shown. * $p < 0.05$, ** $p < 0.005$, *** $p < 0.0005$, and **** $p < 0.0001$.

(C) H mAb competition with SLAMF1-huFC using H- or F-expressing 293T cells (or untransfected cells), measured with flow cytometry. F-specific mAb 3A12 and "no-mAb" treatments were included as controls. The (top) shows average mAb-cell surface binding levels quantified as percentage mAb+ cells. The (bottom) shows average SLAMF1-huFC binding levels quantified as percentage SLAMF1+ cells. **** $p < 0.0001$.

(D) F_{ECT} thermal unfolding with and without Fabs measured using intrinsic fluorescence at 330 nm. Shown are nannoDSF 1st derivative traces of Fab-F_{ECT} complexes from 25°C to 100°C. F_{ECT} alone is shown in gray, Fabs alone are shown in black, and complexes are color coded by Fab.

See also Figure S4.

For F-specific mAbs, ADCC activity tended to be high in mAbs with good neutralization and protection. Interestingly, ADCP activity for these mAbs does not forecast protection, but instead, inversely correlates with neutralization and protection (Figure S4F). Further, highly protective antibody 4F09 does not exhibit high levels of either Fc function tested, thus it may provide protection via mechanical neutralization alone. Together, these data suggest that neutralization is the primary driver of protection for these anti-H and anti-F mAbs, with Fc functions contributing variably.

In vivo mAb therapeutic protection and *in vitro* cross-reactivity

We examined the therapeutic efficacy of mAbs 4D08, 1C08, 3A12, and 4F09 in cotton rats when administered 24 or 48 h after MeV infection (Figure 5A). All mAbs significantly reduced

Please cite this article in press as: Acciani et al., Human neutralizing antibodies targeting the measles virus hemagglutinin and fusion surface proteins, Cell Host & Microbe (2026), https://doi.org/10.1016/j.chom.2026.04.010

CellPress
OPEN ACCESS

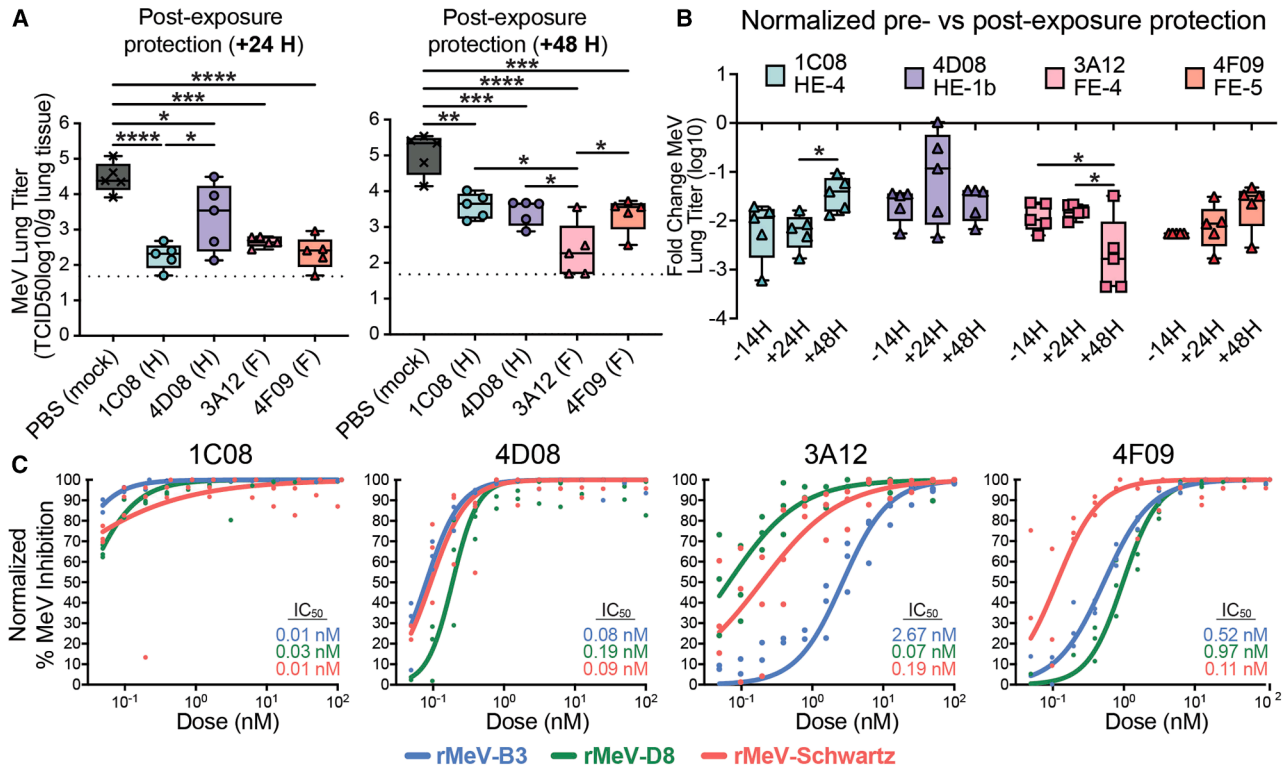

Figure 5. Post-exposure efficacy and neutralization breadth for protective MeV mAbs

(A) Cotton rats were inoculated with 2×10^5 $TCID_{50}$ rMeV-B3-GFP, then injected with each mAb (1 mg/kg, 5 animals per mAb) or PBS (5 animals) at 24 (+24H) or 48 (+48H) h after infection. 4 days after infection, lung tissue homogenates were prepared and titrated on Vero-SLAMF1 cells. Minimum, median, and maximum viral titers ($TCID_{50}$log10/g lung tissue) are shown using box and whisker plots; * $p < 0.05$, ** $p < 0.005$, *** $p < 0.0005$, and **** $p < 0.0001$ by one-way ANOVA multiple comparisons test with Tukey's correction.

(B) Pre- and post-exposure mAb treatments were normalized by calculating the fold-change in viral lung titers in mAb-treated animals versus control animals, per mAb per treatment regimen. Minimum, median, and maximum viral titer differences are shown using box and whisker plots. Treatment regimens (−14H, +24H and +48H) were compared for each mAb; * $p < 0.05$, ** $p < 0.005$, *** $p < 0.0005$, and **** $p < 0.0001$.

(C) MAbs (0.05 to 100 nM) and rMeV-B3, rMeV-D8, or rMeV-Schwartz (200–300 plaque-forming units [pfu]/well) were applied to vero-SLAMF1 cells to assess mAb neutralization efficiencies. After 48 h, mCherry-infected cells were quantified using a Cytation 5 (BioTek). For each mAb at each dilution, percentage MeV inhibition was calculated and normalized using no-mAb in infected wells. Shown are the normalized data points from three independent experiments and nonlinear regression curves fit to the data to determine the IC_{50} for each mAb.

lung MeV titers, with mAb 3A12, interestingly, performing best 48 h after infection (Figure 5B). MAbs 4D08 and 4F09 maintained similar levels of efficacy across treatment regiments, while mAb 1C08 therapeutic efficacy decreased 48 h after infection.

All MeVs sequenced from confirmed cases in the Americas in 2025 were identified as either genotype B3 or D8. We tested mAb *in vitro* neutralization of an MeV encoding H and F from B3 (rMeV-B3) or D8 (rMeV-D8) viruses, compared to a virus encoding the Schwartz/Moraten vaccine strain (rMeV-Schwartz) (Figure 5C). H mAbs 1C08 and 4D08 potently neutralized all viruses with picomolar efficacy. Anti-F mAb 4F09 inhibited rMeV-Schwartz 5–9 times more effectively than either circulating strain but still neutralized currently circulating genotypes with picomolar efficacy (B3 IC_{50} of 520 pM, D8 IC_{50} of 970 pM). MAb 3A12 neutralized rMeV-D8 and rMeV-Schwartz (IC_{50} of 190 pM and 70 pM, respectively) 14–38-fold more efficiently than rMeV-B3 (IC_{50} of 2,670 pM; 2.7 nM), although we note that < 3 nM neutralization is still highly potent.

Cryo-EM analysis of H and F complexed with protective Fabs

To reveal antibody contacts that confer *in vivo* protection, we resolved cryo-electron microscopy (cryo-EM) structures of MeV H_{ECT} and F_{ECT} complexed with Fab fragments of the protective anti-H mAbs 1C08 and 4D08 and anti-F mAbs 4F09 and 3A12 (Figures 6, 7, and S5; Tables S2 and S3).

H structures

Cryo-EM reconstructions of H_{ECT}-Fab complexes reveal that H_{ECT} retains a homodimeric state throughout purification and structural analysis (Figures 6 and S5; Data S3). The globular head domains within the dimer are tilted 60° relative to each other, and glycan moieties are visible at N200, N215, and N416, which is consistent with prior structural data.[7,8,38,44]

Anti-H antibody 1C08

Cryo-EM of H_{ECT} complexed with Fab 1C08 (3.2 Å), epitope group HE-4 (cyan, Figures 6A–6C), shows that this mAb anchors symmetrically to the peripheral undersides of the H dimer. The 1C08 heavy chain predominately mediates H binding through four hydrogen bonds and one salt bridge. Binding of 1C08

Please cite this article in press as: Acciani et al., Human neutralizing antibodies targeting the measles virus hemagglutinin and fusion surface proteins, Cell Host & Microbe (2026), https://doi.org/10.1016/j.chom.2026.04.010

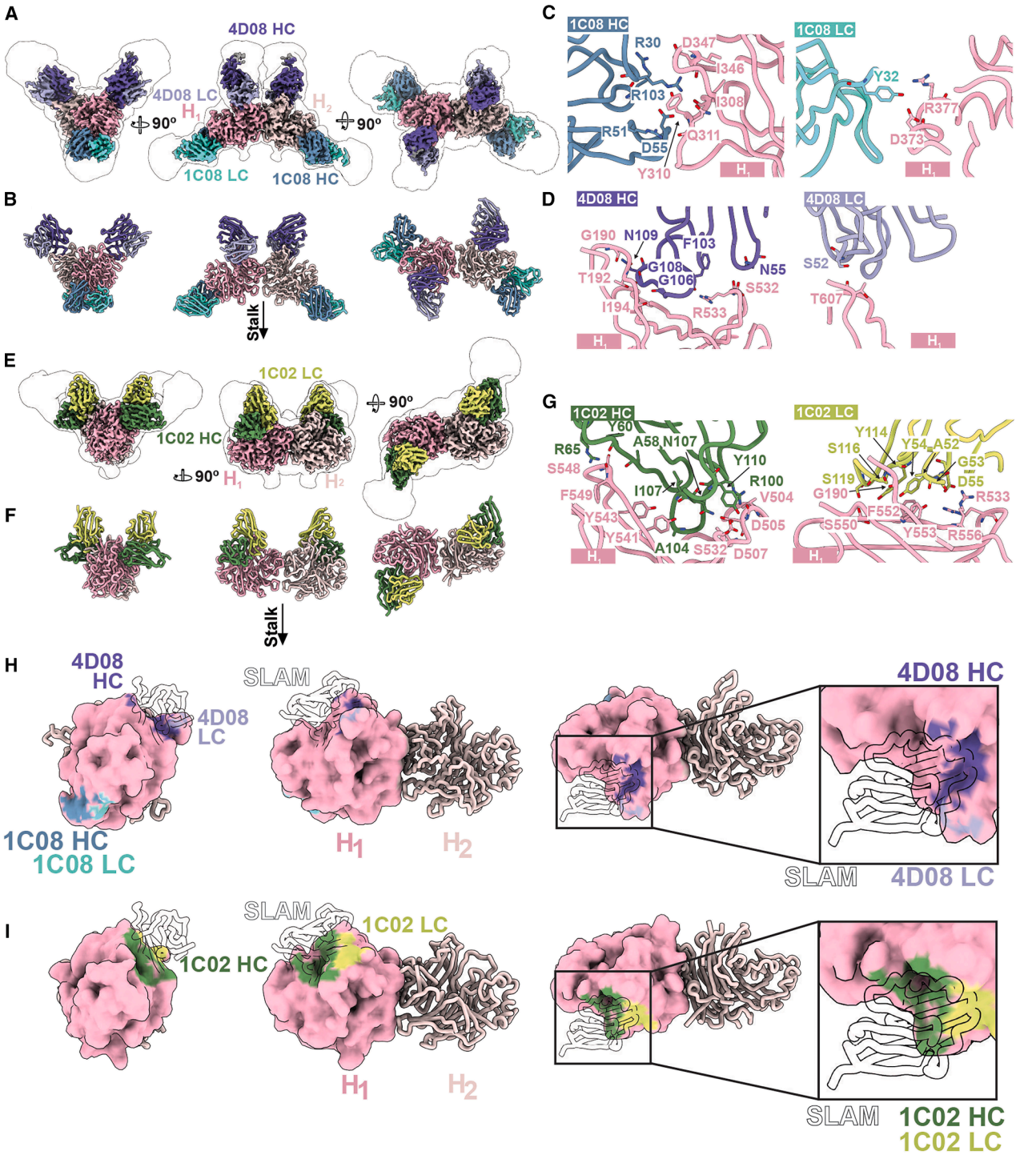

Figure 6. Cryo-EM structures of MeV H_{ECT} in complex with neutralizing antibodies

H_{ECT} monomers (pink shades) in complex with 4D08, 1C08, and 1C02 Fab fragments. The stalk is indicated by an arrow denoting the membrane-proximal orientation. The low-pass filtered cryo-EM maps (at 1.5 standard deviations) are outlined to provide contextual density.

(A) Cryo-EM density map H_{ECT} in complex with Fabs 4D08 (purple) and 1C08 (blue).

(B) Atomic model corresponding to (A), shown as ribbons.

(C) Detailed view of the interaction interfaces between the heavy (left, dark blue) and light (right, cyan) chains of 1C08 and H_{ECT} (pink).

(D) Interaction interfaces between the heavy (left, dark purple) and light (right, lavender) chains of 4D08 and H_{ECT}.

(E) Cryo-EM density map of H_{ECT} bound to mAb 1C02.

(F) Corresponding ribbon model of the complex shown in (C).

(legend continued on next page)

Please cite this article in press as: Acciani et al., Human neutralizing antibodies targeting the measles virus hemagglutinin and fusion surface proteins, Cell Host & Microbe (2026), https://doi.org/10.1016/j.chom.2026.04.010

CellPress
OPEN ACCESS

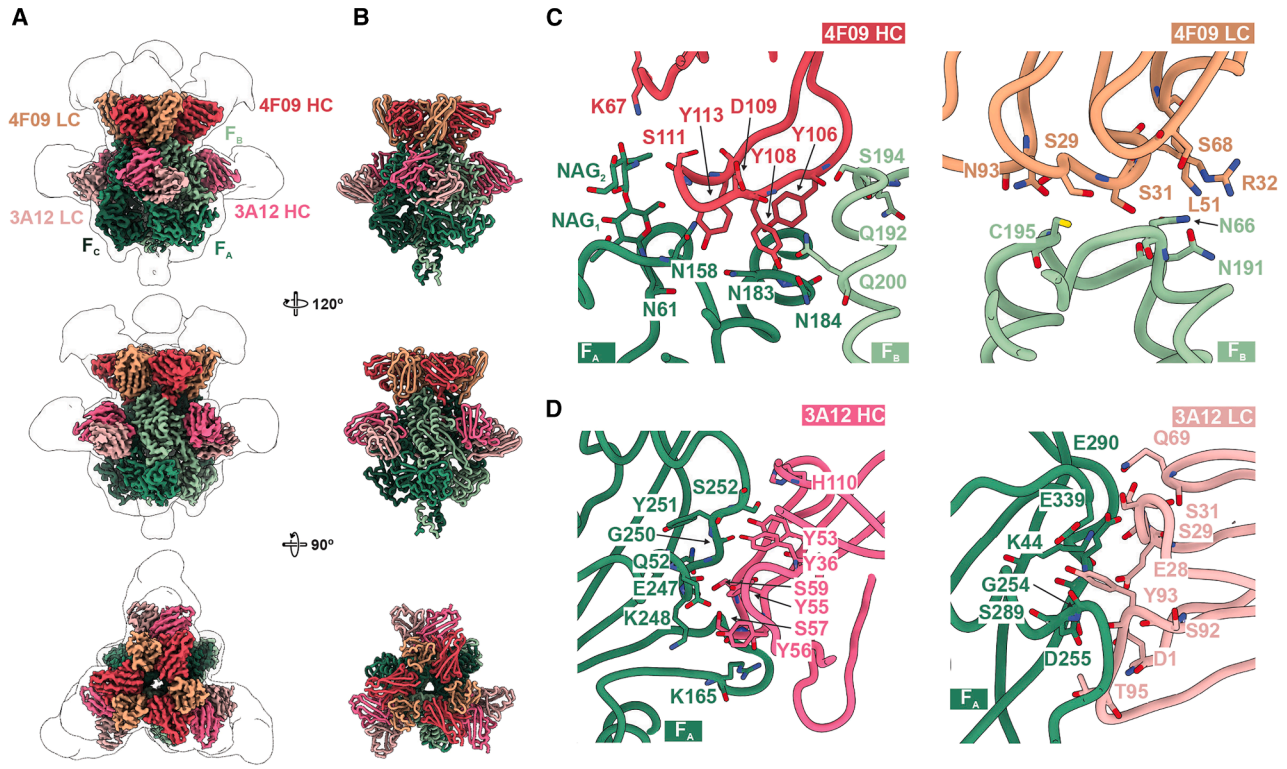

Figure 7. Cryo-EM structures of MeV F_{ECT} in complex with neutralizing antibodies 4F09 and 3A12.

F_{ECT} protomers are shown in green, with Fab heavy and light chains distinguished by complementary colors. NAG denotes N-acetylglucosamine moieties.

(A) Cryo-EM density map of F_{ECT} in complex with 4F09 and 3A12 Fabs, shown from three orthogonal views. The map outline represents a low-pass filtered density contoured at 1.5 standard deviations.

(B) Corresponding ribbon models of the complex shown in (A). F protomers are labeled F_A, F_B, and F_C.

(C) Close-up views of the interface between 4F09 and F_{ECT}. (Left) 4F09 heavy chain (red) engaging two protomers (F_A and F_B), including interactions with glycans from N-glycosylated N61. (Right) 4F09 light-chain (orange) interactions with the F_B protomer.

(D) Close-up views of the interface between 3A12 and F_{ECT}. (Left) 3A12 heavy chain (magenta) binding a single protomer (F_A), engaging both F1 and F2 fragments. (Right) 3A12 light-chain (light pink) interaction with F_A, forming extensive contacts across the surface.

See also Figures S3, S5, and S7; Tables S2 and S3; and Data S4.

fosters little structural change in the H dimer structure (using reference apo structure 2RKC[44]), with a minor, 1.3 Å conformational shift in a loop containing residue 311 away from the antibody paratope.

Anti-H antibody 4D08

We solved a complex of H_{ECT} with 4D08 and 1C08 to mitigate preferred orientation and obtained a high-resolution reconstruction (3.3 Å) (Figures 6A, 6B, and 6D). 4D08 symmetrically engages epitope HE-1b on the apical surface of each monomer in the dimer, primarily through a flattened loop in the CDR H3 (residues 103–109) that occupies a crevice formed by blades β1 and β5 of H, much like the interaction mediated by SLAMF1 residues 127–133 (Figure 5F).[7,38]

Binding of 4D08 induces structural remodeling in H propagating from blade β5 strand β4 residues S544 to I564 (Figure S6A). 4D08 recognition of H β5 loop P545–R547 draws this loop ~3.5 Å outward, pulling residues S544–P545 out of register (Figures S6B and S6C). The surrounding β strands accommodate this register shift, likely due to sequence similarity between the unshifted and shifted regions, allowing for local reorganization of the H fold.

Anti-H antibody 1C02

We also solved the structure of non-protective HE-1a Fab 1C02 (3.1 Å) (Figures 6E–6G), revealing that this Fab engages the receptor-binding groove extensively and overlaps six SLAMF1 contact residues (D507, S532, R533, F552, Y553, and R556), one nectin-4 contact residue (F549), and five multi-receptor contact residues (D505, Y541, Y543, S548, and S550).[38]

1C02 also induces a register shift in H blade β5 strand β4 residues 546–555 (Figure S6C, center right). In the 1C02 complex, six loops containing residues Q248, F284, D342, K460, V534, and S590 adopt alternate conformations relative to the apo structure. Additionally, the antibody loop containing S117 (CDR L3) introduces steric hindrance with H_{ECT}, causing structural

(G) Interaction interfaces between the heavy (left, green) and light (right, yellow) chains of 1C02 and H_{ECT}.

(H and I) Footprints of 1C08 and 4D08 (H) and 1C02 (I) Fabs mapped on H_{ECT} surfaces by coloring surface residues within 3 Å of each Fab. H1 is illustrated as a molecular surface and H_2 as a C alpha trace. Footprints by chain are colored as in (A–G).

See also Figures S3 and S5–S7; Tables S2–S4; and Data S3.

Please cite this article in press as: Acciani et al., Human neutralizing antibodies targeting the measles virus hemagglutinin and fusion surface proteins, Cell Host & Microbe (2026), https://doi.org/10.1016/j.chom.2026.04.010

rearrangement of the N- and C-terminal β sheets of the β-propeller fold (blades β1 and β6, residues S189–S199 and H593–C606).

The 4D08/1C02-induced register shift in H mimics conformational changes previously reported in H-SLAMF1 complexes (PDB: 3ALW, 3ALX, 3ALZ) but absent in H-nectin-4 (PDB: 4GJT) and H-CD46 (PDB: 3INB) complexes. Thus, 1C02 and 4D08 may mimic receptor-induced conformational states or were elicited against an H structure resembling that of the receptor-bound form.

The 4D08 (HE1b) and 1C02 (HE1a) epitopes are uniquely positioned with respect to the receptor-binding groove (Figures 6H and 6I). 1C02 more extensively interacts with the inside of this groove, contacting 15 H residues in the anterior wall and throughout the inside of the cavity. Five of these residues are critical for SLAMF1 recognition (D505, D507, R533, F552, Y553).[45,46] Meanwhile, 4D08 binds to fewer, more surface-accessible residues along the walls and edges of the cavity, and four 4D08 contact residues (T192, I194, S532, and R533) are also involved in SLAMF1 interactions.

F structures

We resolved the cryo-EM structure of a 3A12 (HE-4)-, 4F09 (HE-5)-F ternary complex at 2.3 Å resolution (Figures 7 and S5; Data S4). Both 3A12 and 4F09 are attached at full occupancy, with three copies of each Fab per F trimer.

3A12 binds to the center of each protomer face, engaging F extensively across the F1 and F2 subunits (Figures 7A, 7B, and 7D). 3A12 binding causes a ~3.0 Å conformational shift in F residues G250–G254, but otherwise the structure of bound and unbound F_{ECT} are similar at the 3A12 epitope, with a root-mean-square deviation (RMSD) of 0.7 Å.

4F09 binds to the F apex, where each Fab simultaneously engages two F protomers (Figures 7A–7C). The 4F09 CDR H3 contains an 8-residue tyrosine-rich (4 Tyr among 8 residues) loop from Y106 to Y113 that interacts with the F1 DIII domains of two protomers simultaneously, and the HR-N (F1) and N61 glycan (F2) in a single protomer.

H epitope conservation

Use of mAbs in prophylaxis or treatment requires recognition of conserved residues. Analysis of 2,350 H sequences and 1,436 F sequences from the NCBI Protein Databank[47] (Figures S7A and S7B; Table S2) showed that highly protective mAb 1C08 (HE-4) has a broadly conserved epitope and would likely have robust activity against circulating variants (Figure S7A_I). 1C08 forms key hydrogen bonds to the side chains of fully or highly conserved residues D347, D373, and D377 (99.96%–100% conserved), and backbone-only interactions to four moderate-to-highly conserved residues I308, Y310, Q311, and I346 (84%–99% conserved). The least conserved residue I346 (84%) exists as V346 in circulating B3 strains; however, this I to V side-chain change would most likely not impact 1C08 recognition as it binds backbone-only at this site.

MAb 4D08 (HE-1b) also binds to a highly conserved region on H. Only one residue, S532, has a database variant (S532F) that might impact side-chain-mediated interactions (Figure S7A_{II}). Notably, this variant occurs once in 2,350 sequences, and S532 is implicated in SLAMF1 binding.[38]

Less-protective mAb 1C02 (HE-1a) binds to a larger epitope that, while highly conserved (98.26%–100% conservation), may be more susceptible to escape mutations (Figure S7A_{III}). Key contact residues with reported variations include D505 (D505G/Y), Y541 (Y541N), Y543 (Y543H), and S532 (S532F), all of which form side-chain hydrogen bonds to 1C02. While these mutations occur at low frequencies (1 to 4 instances out of 2,305 sequences), they suggest a slightly higher susceptibility of 1C02 to escape mutations compared with mAbs 1C08 and 4D08. Variants S532F, Y541N, and Y543H were found in clinical isolates,[48–51] while D505G/Y was found exclusively in vaccine or other lab-adapted strains.[52–54]

F epitope conservation

The highly protective 3A12 (FE-4, protomer face) contacts 16 residues, 15 of which are 99.4%–100% identical across all 1,436 known F sequences (Figure S7B_I). The sixteenth residue, G254, is 85.5% conserved among all historical sequences but 100% conserved among currently circulating strains (genotypes B3 and D8). Finally, the highly protective 4F09 (FE-5) exclusively contacts residues that are each 99.6%–100% identical among all sequences (Figure S7B_{II}).

DISCUSSION

The live-attenuated MeV vaccine confers lifelong, durable protection against disease in 90%–99% of vaccinees, but the antibody responses it elicits remained unclear.[55,56] We evaluated 15 Measles-Mumps-Rubella (MMR)-vaccinated donors for their polyclonal MeV responses to identify individuals with vaccine-induced, protective, circulating antibodies.

One individual, a 56-year-old female, who was vaccinated in childhood and boosted five years before sample collection, demonstrated the highest polyclonal response and the most H- and F-reactive memory B cells. About 1% of her total circulating B cells were directed against MeV F, while ~0.5% were against H, figures similar to previous reports of human polyclonal sera.[13,57]

This individual's PBMCs were used for mAb discovery using an optofluidic strategy and recombinant, fully glycosylated H_{ECT} and F_{ECT} antigens. Hundreds of B cell clones against H_{ECT} and F_{ECT} were identified and used to engineer, express, and purify approximately 50 mAbs per antigen. MAbs were sorted into competition groups and assigned to epitopes HE1-4 or FE1-5.

MeV H epitopes

Of the mAbs targeting the H-receptor-binding groove (epitopes HE-1 and HE-2), only HE-1b mAb 4D08 directly inhibits SLAMF1 binding, neutralizes viruses *in vitro* (IC_{50} 0.149 nM), and protects *in vivo*. HE-1a mAb 1C02 also blocks SLAMF1, neutralized viruses, and induces similar, receptor-like conformational changes in H upon binding, yet requires a 5× higher dose to protect prophylactically in the cotton rat model. Further investigation is required to test whether the *in vivo* efficacies of these mAbs vary due to differences in epitope footprint, Fc function, or pharmacokinetics.

HE-4 mAb 1C08, which works against the H periphery, does not block receptor recognition or alter the H dimer upon binding, yet exhibits picomolar viral neutralization and protects *in vivo*. The position of this epitope, combined with cryo-EM modeling of the H-F interaction of the related human parainfluenza virus 3,[58] suggests that 1C08 may prevent MeV H and F interactions.

H contacts for mAbs 4D08 (receptor-binding site) and 1C08 (H periphery) are highly conserved, particularly in currently

Please cite this article in press as: Acciani et al., Human neutralizing antibodies targeting the measles virus hemagglutinin and fusion surface proteins, Cell Host & Microbe (2026), https://doi.org/10.1016/j.chom.2026.04.010

circulating MeV genotypes. Importantly, no H contact residue identified for 1C08 or 4D08 is a positive selection site in MeV H evolution.[59,60] Furthermore, both mAbs neutralize MeVs bearing genotypically diverse glycoproteins with similar, nanomolar efficacies, and significantly reduce MeV titers in cotton rats when administered 24 to 48 h after virus inoculation.

MeV F epitopes

MAb F epitopes FE-1 through FE-5 encompass most of the F trimer surface, from the membrane-proximal pyramid base to the trimer apex. MAbs targeting the trimer's upper half and apex (FE-3, -4, and -5) universally neutralize with an IC_{50} of at least 0.192 nM and significantly reduce MeV lung titers in cotton rats when administered prophylactically. Those against the bottom half of F (epitope groups FE-1 and -2) neutralize poorly and are not protective. We find that the most protective anti-F antibodies in this study, 3A12 (FE-4) and 4F09 (FE-5), significantly increase the thermal stability of the F prefusion trimer. These mAbs bind conformational, quaternary epitopes spanning both F1 and F2 subunits together, likely anchoring them together and preventing the major conformational rearrangements required for fusion.

We find abundant antibodies against F in this study (twice as many as against H), including mAbs that neutralize potently and fully protect in the cotton rat model. Anti-F antibody 3A12 was the most effective therapeutic mAb included in this study, reducing MeV lung titers 500-fold when administered 24 to 48 h after infection. These findings contrast with the historical notion that neutralization is associated mainly with H. Here, we specifically selected B cells using an F that was engineered to preserve the prefusion conformation,[34] whereas earlier studies were performed using vaccine-sequence F.[22,26,37,61–72] Our use of prefusion F to identify antibodies likely favored identification of neutralizing antibodies, especially those that neutralize by preventing the conformational rearrangements associated with membrane fusion. However, we note that the mAbs in our study are from one individual with high circulating anti-MeV-H/F IgG and may not be representative of the average response to vaccination.

Comparing these antibodies to previous work

Now that we have 3D structural information for the landscape of H and F recognition, we can reconcile studies performed prior to the availability of antibody structures (Figures S7C and S7D). Previous work used competition assays to assign neutralizing murine mAbs to epitope groups (mostly against H) and incorporated data from pepscans[73] and virus resistance escape sequencing to approximate the epitope locations.[14,17,74,75] Here, we finely binned H- and F-specific neutralizing and non-neutralizing human mAbs into competition groups, solved 3D structures, and provided evidence linking epitopes to therapeutic efficacy *in vivo*. For H, residues previously clustered into groups III and the "noose" generally map to epitope groups HE-1a/1b and HE-2a/b, respectively, while residues in murine group Ia map to epitope group HE-4 (Figure S7C; Table S4). For F, previously implicated residue R73[27] maps to human epitope footprint FE-3, residues G240-258[76] to FE-4, and residues A388 and C420[25,28,77,78] to FE-1a/b (Figure S7B).

Our group recently resolved structures of murine F mAbs in complex with prefusion F (Data S4).[43] Like 4F09, murine mAb Y10F targets the trimer apex and stabilizes the prefusion trimer. Both mAbs are similarly protective prophylactically, and 4F09 maintains efficacy when administered up to 48 h after infection (not yet evaluated for Y10F). FE-4 mAb 3A12 binds to an epitope on the upper face of the trimer and also inhibits F by locking the trimer in the prefusion state (more effectively than any other anti-F mAb, as measured by prefusion F thermal stability). Murine mAb-77,[34,43] which traps F in a fusion-intermediate state, shares an epitope with human mAb 2G05 (FE-2); however, mAb-77 is a more effective neutralizer and a more potent inhibitor *in vivo*. Murine mAb H8,[43] which binds an epitope on the lower trimer face opposite from FE-2, prematurely activates F into springing to the post-triggered state. The H8 epitope resembles that of HE-1a mAb 2D07, and both mAbs moderately neutralize viruses and do not protect prophylactically. Further characterization is required to determine whether mAb 2D07 also induces prefusion triggering. Combined, these studies illustrate three distinct mechanisms of F inhibition: premature activation of F, stabilization of the prefusion state, and stabilization of a fusion-intermediate state; with evidence suggesting that the latter two mechanisms are more effective at inhibiting virus *in vivo*.

The therapeutic potential of anti-measles mAbs

Compassionate use of mAb m102.4[79] against Hendra virus, and recent FDA approval of nirsevimab[80] and clesrovimab[81] against the related respiratory syncytial virus (RSV), open the door to use of mAbs against MeV. Such use of recombinant human mAbs for pre- or post-exposure therapy against MeV is of high interest as cases rise and outbreaks become more frequent. Here, we identified four potent, fully human mAbs against MeV H and F that exhibit picomolar neutralization and deliver effective prophylactic *and* therapeutic protection against MeV in the cotton rat model. Further safety and efficacy preclinical and clinical evaluations are now needed. The relationship between cotton rat MeV lung titers and human MeV disease outcomes has not yet been examined; however, studies evaluating anti-RSV mAbs suggest that this model is highly valuable at predicting the dose and efficacy of antibody treatments in children.[82]

Antibodies against MeV would be particularly useful in the immunocompromised and people not yet fully vaccinated, including small children too young to be vaccinated. Indeed, subacute sclerosing panencephalitis, a progressive and nearly always fatal complication of measles infection, occurs more often in children infected before age 2.[83] These populations currently have no options beyond reliance on herd immunity. Monoclonal antibodies may finally provide a complementary protective or therapeutic option. The protective mAbs identified here target four distinct, non-competing epitopes, and may be combined as cocktail therapies to enhance treatment potency, maintain durable protection, and reduce the risk of viral escape.

Although the MMR vaccine has been widely used since its introduction in 1963, and has saved an estimated 94 million lives, human antibodies elicited by this vaccine were poorly understood. This study maps the landscape of antibody recognition against MeV in a human vaccinee (with unknown exposure to wild-type virus), and illuminates recognition sites on both H and F antigens that lead to *in vitro* neutralization and *in vivo* prophylactic and therapeutic protection. Further, these human mAbs themselves, which recognize conserved sites and inhibit

measles by complementary mechanisms, represent a basis to develop a treatment that is urgently needed as measles virus infections surge globally.

RESOURCE AVAILABILITY

Lead contact

Further information and requests for resources and reagents should be directed to and will be fulfilled by the lead contact, Erica Ollmann Saphire (erica@lji.org).

Materials availability

All reagents generated in this study are available from the lead contact upon request with a materials transfer agreement.

Data and code availability

Datasets generated during this study are included in the article or are available from the corresponding authors on request. Negative-stain electron microscopy (NS-EM) maps and cryo-EM structures of MeV H_{ECT} and F_{ECT} in complex with mAbs are available through the EMDB (https://www.ebi.ac.uk/emdb) and PDB (https://www.rcsb.org) repositories. Accession numbers are listed in the key resources table.

This paper does not report any original code.

Any additional information required to reanalyze the data reported in this paper is available from the lead contact upon request.

ACKNOWLEDGMENTS

The authors thank Ruben Diaz Avalos of the La Jolla Institute for Immunology Cryo-EM facility and Cheryl Kim of the flow cytometry core for assistance with data collection; and the GHR Foundation and private donors for support of instrumentation. We also thank Dr. Sharon Schendel for critical revision of the manuscript. Molecular graphics were performed with UCSF ChimeraX, developed by the Resource for Biocomputing, Visualization, and Informatics at the University of California, San Francisco, with support from National Institutes of Health R01-GM129325 and the Office of Cyber Infrastructure and Computational Biology, National Institute of Allergy and Infectious Diseases. This work was supported by the National Institutes of Health (NIH R21 AI180456 [E.O.S.]); Swiss National Science Foundation Postdoc Mobility fellowships P2EZP3_195680 (D.Z.) and P500PB_210992 (D.Z.); NIAID R56AI183536, R01AI190902, and R01AI195589 (M.P. and E.O.S.); NINDS R01NS105699 (M.P.), and institutional funds of La Jolla Institute for Immunology (E.O.S.).

AUTHOR CONTRIBUTIONS

Conceptualization, M.A., D.Z., and E.O.S.; methodology, S.H., D.Z., S.N., M.E.A., M.P., and K.M.H.; investigation, M.A., D.Z., G.N., S.H., D.P., E.P., D.L., D.K., S.N., M.P., and K.M.H.; formal analysis, M.A., D.Z., G.N., E.P., D.L., S.N., M.P., M.E.A., and K.M.K.; data curation, M.A. and D.Z.; resources, D.P., M.P., S.N., M.E.A., and E.O.S.; visualization, M.A. and D.Z.; supervision, M.P., M.E.A., S.N., K.M.K. and E.O.S; project administration, E.O.S.; funding acquisition, E.O.S. and M.P.; writing (original draft), M.A., D.Z., and E.O.S; and writing (review and editing), M.A., D.Z., M.E.A., M.P., S.N., K.M.H., and E.O.S.

DECLARATION OF INTERESTS

The antibodies and stabilized F discussed in this manuscript are described in provisional patents. E.O.S. is a member of the advisory boards for *Cell* and *Cell Host Microbe*.

STAR★METHODS

Detailed methods are provided in the online version of this paper and include the following:

- KEY RESOURCES TABLE
- EXPERIMENTAL MODEL AND STUDY PARTICIPANT DETAILS
  - Human sample donation
  - Plasmids
  - Cell lines
- METHOD DETAILS
  - MeV antigen and receptor production and purification
  - Virus
  - Serum ELISAs
  - MeV memory B cell detection via flow cytometry
  - mAb identification and production
  - High-throughput SPR binding kinetics
  - High-throughput SPR epitope binning
  - Epitope mapping using NS-EM
  - AlphaFold3 modeling of antibody-antigen complexes
  - *In vitro* viral neutralization of rMeV-B3-mcherry
  - *In vitro* viral neutralization of MeV genotypes B3, D8, and the Schwartz vaccine strain
  - *In vivo* mAb prophylactic and therapeutic protection in cotton rats
  - mAb/SLAMF1-huFC competition assay
  - Measuring H/F thermal stability using nanoDSF
  - mAb Fc effector function analyses
  - Sample vitrification for Cryo-EM
  - Data acquisition, processing, and model building
  - Structural analysis
  - Sequence conservation analysis
- QUANTIFICATION AND STATISTICAL ANALYSES
  - Sequence analyses
  - *In vitro* neutralization of rMeV-B3-mCherry
  - *In vitro* viral neutralization of MeV genotypes B3, D8, and the Schwartz vaccine strain
  - *In vivo* mAb prophylactic and therapeutic protection in cotton rats
  - mAb/SLAMF1-huFC competition assay

SUPPLEMENTAL INFORMATION

Supplemental information can be found online at https://doi.org/10.1016/j.chom.2026.04.010.

Received: September 18, 2025
Revised: February 12, 2026
Accepted: April 9, 2026

REFERENCES

1. CDC. (2024). Measles Symptoms and Complications. Measles (Rubeola). https://www.cdc.gov/measles/signs-symptoms/index.html.
2. Ferren, M., Horvat, B., and Mathieu, C. (2019). Measles encephalitis: Towards new therapeutics. Viruses *11*, 1017. https://doi.org/10.3390/v11111017.
3. Laksono, B.M., de Vries, R.D., Verburgh, R.J., Visser, E.G., de Jong, A., Fraaij, P.L.A., Ruijs, W.L.M., Nieuwenhuijse, D.F., van den Ham, H.-J., Koopmans, M.P.G., et al. (2018). Studies into the mechanism of measles-associated immune suppression during a measles outbreak in the Netherlands. Nat. Commun. *9*, 4944. https://doi.org/10.1038/s41467-018-07515-0.
4. Mina, M.J., Kula, T., Leng, Y., Li, M., de Vries, R.D., Knip, M., Siljander, H., Rewers, M., Choy, D.F., Wilson, M.S., et al. (2019). Measles virus infection diminishes preexisting antibodies that offer protection from other pathogens. Science *366*, 599–606. https://doi.org/10.1126/science.aay6485.
5. CDC. (2024). Genetic Analysis of Measles Viruses. Measles (Rubeola). https://www.cdc.gov/measles/php/laboratories/genetic-analysis.html.
6. Brindley, M.A., and Plemper, R.K. (2010). Blue native PAGE and biomolecular complementation reveal a tetrameric or higher-order oligomer organization of the physiological measles virus attachment protein H. J. Virol. *84*, 12174–12184. https://doi.org/10.1128/JVI.01222-10.

7. Hashiguchi, T., Ose, T., Kubota, M., Maita, N., Kamishikiryo, J., Maenaka, K., and Yanagi, Y. (2011). Structure of the measles virus hemagglutinin bound to its cellular receptor SLAM. Nat. Struct. Mol. Biol. *18*, 135–141. https://doi.org/10.1038/nsmb.1969.

8. Hashiguchi, T., Kajikawa, M., Maita, N., Takeda, M., Kuroki, K., Sasaki, K., Kohda, D., Yanagi, Y., and Maenaka, K. (2007). Crystal structure of measles virus hemagglutinin provides insight into effective vaccines. Proc. Natl. Acad. Sci. USA *104*, 19535–19540. https://doi.org/10.1073/pnas.0707830104.

9. Santiago, C., Celma, M.L., Stehle, T., and Casasnovas, J.M. (2010). Structure of the measles virus hemagglutinin bound to the CD46 receptor. Nat. Struct. Mol. Biol. *17*, 124–129. https://doi.org/10.1038/nsmb.1726.

10. Lin, L.-T., and Richardson, C.D. (2016). The host cell receptors for measles virus and their interaction with the viral hemagglutinin (H) protein. Viruses *8*, 250. The host cell receptors for measles virus and their interaction with the viral hemagglutinin (h) Lin, L.-T., and Richardson, C.D. (2016).. https://doi.org/10.3390/v8090250

11. Plattet, P., Alves, L., Herren, M., and Aguilar, H.C. (2016). Measles virus fusion protein: Structure, function and inhibition. Viruses *8*, 112. https://doi.org/10.3390/v8040112.

12. Haralambieva, I.H., Kennedy, R.B., Ovsyannikova, I.G., Schaid, D.J., and Poland, G.A. (2019). Current perspectives in assessing humoral immunity after measles vaccination. Expert Rev. Vaccin. *18*, 75–87. https://doi.org/10.1080/14760584.2019.1559063.

13. de Swart, R.L., Yüksel, S., and Osterhaus, A.D.M.E. (2005). Relative contributions of measles virus hemagglutinin- and fusion protein-specific serum antibodies to virus neutralization. J. Virol. *79*, 11547–11551. https://doi.org/10.1128/JVI.79.17.11547-11551.2005.

14. Bouche, F.B., Ertl, O.T., and Muller, C.P. (2002). Neutralizing B cell response in measles. Viral Immunol. *15*, 451–471. https://doi.org/10.1089/088282402760312331.

15. Haralambieva, I.H., Simon, W.L., Kennedy, R.B., Ovsyannikova, I.G., Warner, N.D., Grill, D.E., and Poland, G.A. (2015). Profiling of measles-specific humoral immunity in individuals following two doses of MMR vaccine using proteome microarrays. Viruses *7*, 1113–1133. https://doi.org/10.3390/v7031113.

16. de Swart, R.L., Yüksel, S., Langerijs, C.N., Muller, C.P., and Osterhaus, A.D.M.E. (2009). Depletion of measles virus glycoprotein-specific antibodies from human sera reveals genotype-specific neutralizing antibodies. J. Gen. Virol. *90*, 2982–2989. https://doi.org/10.1099/vir.0.014944-0.

17. Muñoz-Alía, M.Á., Nace, R.A., Zhang, L., and Russell, S.J. (2021). Serotypic evolution of measles virus is constrained by multiple co-dominant B cell epitopes on its surface glycoproteins. Cell Rep. Med. *2*, 100225. https://doi.org/10.1016/j.xcrm.2021.100225.

18. Norrby, E., and Gollmar, Y. (1975). Identification of measles virus-specific hemolysis-inihibiting antibodies separate from hemagglutination-inhibiting antibodies. Infect. Immun. *11*, 231–239. https://doi.org/10.1128/iai.11.2.231-239.1975.

19. Muñoz-Alía, M.A., and Russell, S.J. (2019). Probing morbillivirus antisera neutralization using functional chimerism between measles virus and canine distemper virus envelope glycoproteins. Viruses *11*, 688. https://doi.org/10.3390/v11080688.

20. Muñoz-Alía, M.A., Casasnovas, J.M., Celma, M.L., Carabaña, J., Liton, P.B., and Fernandez-Muñoz, R. (2017). Measles Virus Hemagglutinin epitopes immunogenic in natural infection and vaccination are targeted by broad or genotype-specific neutralizing monoclonal antibodies. Virus Res. *236*, 30–43. https://doi.org/10.1016/j.virusres.2017.04.018.

21. Muñoz-Alía, M.Á., Muller, C.P., and Russell, S.J. (2018). Hemagglutinin-specific neutralization of subacute sclerosing panencephalitis viruses. PLOS One *13*, e0192245. https://doi.org/10.1371/journal.pone.0192245.

22. Sato, T.A., Fukuda, A., and Sugiura, A. (1985). Characterization of major structural proteins of measles virus with monoclonal antibodies. J. Gen. Virol. *66*, 1397–1409. https://doi.org/10.1099/0022-1317-66-7-1397.

23. Muller, C.P., Handtmann, D., Brons, N.H.C., Weinmann, M., Wiesmüller, K.H., Spahn, G., Wiesneth, M., Schneider, F., and Jung, G. (1993). Analysis of antibody response to the measles virus using synthetic peptides of the fusion protein. Evidence of non-random pairing of T and B cell epitopes. Virus Res. *30*, 271–280. https://doi.org/10.1016/0168-1702(93)90095-5.

24. Wiesmüller, K.H., Spahn, G., Handtmann, D., Schneider, F., Jung, G., and Muller, C.P. (1992). Heterogeneity of linear B cell epitopes of the measles virus fusion protein reacting with late convalescent sera. J. Gen. Virol. *73*, 2211–2216. https://doi.org/10.1099/0022-1317-73-9-2211.

25. Partidos, C.D., Ripley, J., Delmas, A., Obeid, O.E., Denbury, A., and Steward, M.W. (1997). Fine specificity of the antibody response to a synthetic peptide from the fusion protein and protection against measles virus-induced encephalitis in a mouse model. J. Gen. Virol. *78*, 3227–3232. https://doi.org/10.1099/0022-1317-78-12-3227.

26. Malvoisin, E., and Wild, F. (1990). Contribution of measles virus fusion protein in protective immunity: anti-F monoclonal antibodies neutralize virus infectivity and protect mice against challenge. J. Virol. *64*, 5160–5162. https://doi.org/10.1128/jvi.64.10.5160-5162.1990.

27. Fayolle, J., Verrier, B., Buckland, R., and Wild, T.F. (1999). Characterization of a natural mutation in an antigenic site on the fusion protein of measles virus that is involved in neutralization. J. Virol. *73*, 787–790. https://doi.org/10.1128/JVI.73.1.787-790.1999.

28. Atabani, S.F., Obeid, O.E., Chargelegue, D., Aaby, P., Whittle, H., and Steward, M.W. (1997). Identification of an immunodominant neutralizing and protective epitope from measles virus fusion protein by using human sera from acute infection. J. Virol. *71*, 7240–7245. https://doi.org/10.1128/jvi.71.10.7240-7245.1997.

29. Mäkelä, M.J., Norrby, E., and Salmi, A. (1987). Measurement of polypeptide- and antigenic site-specific antibodies to measles virus using a competitive enzyme immunoassay. J. Virol. Methods *16*, 65–74. https://doi.org/10.1016/0166-0934(87)90032-2.

30. Muller, C.P., Schroeder, T., Tu, R., Brons, N.H.C., Jung, G., Schneider, F., and Wiesmüller, K.H. (1993). Analysis of the neutralizing antibody response to the measles virus using synthetic peptides of the haemagglutinin protein. Scand. J. Immunol. *38*, 463–471. https://doi.org/10.1111/j.1365-3083.1993.tb02589.x.

31. Obeid, O.E., Partidos, C.D., and Steward, M.W. (1994). Analysis of the antigenic profile of measles virus haemagglutinin in mice and humans using overlapping synthetic peptides. Virus Res. *32*, 69–84. https://doi.org/10.1016/0168-1702(94)90062-0.

32. Mäkelä, M.J., Lund, G.A., and Salmi, A.A. (1989). Antigenicity of the measles virus haemagglutinin studied by using synthetic peptides. J. Gen. Virol. *70*, 603–614. https://doi.org/10.1099/0022-1317-70-3-603.

33. Mathieu, C., Bovier, F.T., Ferren, M., Lieberman, N.A.P., Predella, C., Lalande, A., Peddu, V., Lin, M.J., Addetia, A., Patel, A., et al. (2021). Molecular features of the measles virus viral fusion complex that favor infection and spread in the brain. mBio *12*, e0079921. https://doi.org/10.1128/mBio.00799-21.

34. Zyla, D.S., Della Marca, R., Niemeyer, G., Zipursky, G., Stearns, K., Leedale, C., Sobolik, E.B., Callaway, H.M., Hariharan, C., Peng, W., et al. (2024). A neutralizing antibody prevents postfusion transition of measles virus fusion protein. Science *384*, eadm8693. https://doi.org/10.1126/science.adm8693.

35. Punjani, A., Rubinstein, J.L., Fleet, D.J., and Brubaker, M.A. (2017). cryoSPARC: algorithms for rapid unsupervised cryo-EM structure determination. Nat. Methods *14*, 290–296. https://doi.org/10.1038/nmeth.4169.

36. Pettersen, E.F., Goddard, T.D., Huang, C.C., Couch, G.S., Greenblatt, D.M., Meng, E.C., and Ferrin, T.E. (2004). UCSF Chimera–a visualization system for exploratory research and analysis. J. Comput. Chem. *25*, 1605–1612. https://doi.org/10.1002/jcc.20084.

37. Giraudon, P., and Wild, T.F. (1981b). Monoclonal antibodies against measles virus. J. Gen. Virol. *54*, 325–332. https://doi.org/10.1099/0022-1317-54-2-325.

38. Zhang, X., Lu, G., Qi, J., Li, Y., He, Y., Xu, X., Shi, J., Zhang, C.W.-H., Yan, J., and Gao, G.F. (2013). Structure of measles virus hemagglutinin bound to its epithelial receptor nectin-4. Nat. Struct. Mol. Biol. *20*, 67–72. https://doi.org/10.1038/nsmb.2432.

39. Pettersen, E.F., Goddard, T.D., Huang, C.C., Meng, E.C., Couch, G.S., Croll, T.I., Morris, J.H., and Ferrin, T.E. (2021). UCSF ChimeraX: Structure visualization for researchers, educators, and developers. Protein Sci. *30*, 70–82. https://doi.org/10.1002/pro.3943.

40. Mathieu, C., Ferren, M., Harder, O., Bovier, F.T., Marcink, T.C., Predella, C., Angius, F., Drew-Bear, J., Dorrello, N.V., Greninger, A.L., et al. (2021). Single-chain variable fragment antibody constructs neutralize measles virus infection in vitro and in vivo. Cell. Mol. Immunol. *18*, 1835–1837. https://doi.org/10.1038/s41423-021-00691-y.

41. Niewiesk, S. (2009). Current animal models: cotton rat animal model. Curr. Top. Microbiol. Immunol. *330*, 89–110. https://doi.org/10.1007/978-3-540-70617-5_5.

42. Carsillo, T., Huey, D., Levinsky, A., Obojes, K., Schneider-Schaulies, J., and Niewiesk, S. (2014). Cotton rat (Sigmodon hispidus) signaling lymphocyte activation molecule (CD150) is an entry receptor for measles virus. PLOS One *9*, e110120. https://doi.org/10.1371/journal.pone.0110120.

43. Zyla, D.S., Della Marca, R., Lacarbonara, D., Niemeyer, G., Zipursky, G., Di Clemente, L., Jonathan-Trakht, G., Kalantarov, G., Acciani, M., Laterza, G., et al. (2026). Structural and mechanistic basis for antibody neutralization of the measles fusion protein. Nat. Comm. Advance online publication. https://doi.org/10.1038/s41467-026-71373-4.

44. Colf, L.A., Juo, Z.S., and Garcia, K.C. (2007). Structure of the measles virus hemagglutinin. Nat. Struct. Mol. Biol. *14*, 1227–1228. https://doi.org/10.1038/nsmb1342.

45. Massé, N., Ainouze, M., Néel, B., Wild, T.F., Buckland, R., and Langedijk, J.P.M. (2004). Measles virus (MV) hemagglutinin: evidence that attachment sites for MV receptors SLAM and CD46 overlap on the globular head. J. Virol. *78*, 9051–9063. https://doi.org/10.1128/JVI.78.17.9051-9063.2004.

46. Vongpunsawad, S., Oezgun, N., Braun, W., and Cattaneo, R. (2004). Selectively receptor-blind measles viruses: Identification of residues necessary for SLAM- or CD46-induced fusion and their localization on a new hemagglutinin structural model. J. Virol. *78*, 302–313. https://doi.org/10.1128/JVI.78.1.302-313.2004.

47. Sayers, E.W., Beck, J., Bolton, E.E., Brister, J.R., Chan, J., Connor, R., Feldgarden, M., Fine, A.M., Funk, K., Hoffman, J., et al. (2025). Database resources of the National Center for Biotechnology Information in 2025. Nucleic Acids Res. *53*, D20–D29. https://doi.org/10.1093/nar/gkae979.

48. Rota, J.S., Rota, P.A., Redd, S.B., Redd, S.C., Pattamadilok, S., and Bellini, W.J. (1998). Genetic analysis of measles viruses isolated in the United States, 1995–1996. J. Infect. Dis. *177*, 204–208. https://doi.org/10.1086/513825.

49. Miki, K., Komase, K., Mgone, C.S., Kawanishi, R., Iijima, M., Mgone, J.M., Asuo, P.G., Alpers, M.P., Takasu, T., and Mizutani, T. (2002). Molecular analysis of measles virus genome derived from SSPE and acute measles patients in Papua, New Guinea. J. Med. Virol. *68*, 105–112. https://doi.org/10.1002/jmv.10176.

50. Ivancic-Jelecki, J., Baricevic, M., Santak, M., Harcet, M., Tešović, G., Marusic Della Marina, B., and Forcic, D. (2013). The first genetic characterization of a D4 measles virus strain derived from a patient with subacute sclerosing panencephalitis. Infect. Genet. Evol. *17*, 71–78. https://doi.org/10.1016/j.meegid.2013.03.032.

51. hemagglutinin [Measles morbillivirus] – Protein (National Center for Biotechnology Information). (n.d.). https://www.ncbi.nlm.nih.gov/protein/ACJ86382.

52. Borges, M.B., Caride, E., Jabor, A.V., Malachias, J.M.N., Freire, M.S., Homma, A., and Galler, R. (2008). Study of the genetic stability of measles virus CAM-70 vaccine strain after serial passages in chicken embryo fibroblasts primary cultures. Virus Genes *36*, 35–44. https://doi.org/10.1007/s11262-007-0173-1.

53. Rota, J.S., Wang, Z.D., Rota, P.A., and Bellini, W.J. (1994). Comparison of sequences of the H, F, and N coding genes of measles virus vaccine strains. Virus Res. *31*, 317–330. https://doi.org/10.1016/0168-1702(94)90025-6.

54. Hummel, K.B., Vanchiere, J.A., and Bellini, W.J. (1994). Restriction of fusion protein mRNA as a mechanism of measles virus persistence. Virology *202*, 665–672. https://doi.org/10.1006/viro.1994.1388.

55. Bitzegeio, J., Majowicz, S., Matysiak-Klose, D., Sagebiel, D., and Werber, D. (2019). Estimating age-specific vaccine effectiveness using data from a large measles outbreak in Berlin, Germany, 2014/15: Evidence for waning immunity. Euro Surveill. *24*, 1800529. https://doi.org/10.2807/1560-7917.ES.2019.24.17.1800529.

56. Franconeri, L., Antona, D., Cauchemez, S., Lévy-Bruhl, D., and Paireau, J. (2023). Two-dose measles vaccine effectiveness remains high over time: A French observational study, 2017–2019. Vaccine *41*, 5797–5804. https://doi.org/10.1016/j.vaccine.2023.08.018.

57. de Swart, R.L., Vos, H.W., UytdeHaag, F.G., Osterhaus, A.D., and van Binnendijk, R.S. (1998). Measles virus fusion protein- and hemagglutinin-transfected cell lines are a sensitive tool for the detection of specific antibodies by a FACS-measured immunofluorescence assay. J. Virol. Methods *71*, 35–44. https://doi.org/10.1016/S0166-0934(97)00188-2.

58. Marcink, T.C., Zipursky, G., Cheng, W., Stearns, K., Stenglein, S., Golub, K., Cohen, F., Bovier, F., Pfalmer, D., Greninger, A.L., et al. (2023). Subnanometer structure of an enveloped virus fusion complex on viral surface reveals new entry mechanisms. Sci. Adv. *9*, eade2727. https://doi.org/10.1126/sciadv.ade2727.

59. Zhou, N., Li, M., Huang, Y., Zhou, L., and Wang, B. (2021). Genetic characterizations and molecular evolution of the measles virus genotype B3's hemagglutinin (H) gene in the elimination era. Viruses *13*, 1970. https://doi.org/10.3390/v13101970.

60. Kimura, H., Saitoh, M., Kobayashi, M., Ishii, H., Saraya, T., Kurai, D., Tsukagoshi, H., Shirabe, K., Nishina, A., Kozawa, K., et al. (2015). Molecular evolution of haemagglutinin (H) gene in measles virus. Sci. Rep. *5*, 11648. https://doi.org/10.1038/srep11648.

61. Birrer, M.J., Bloom, B.R., and Udem, S. (1981). Characterization of measles polypeptides by monoclonal antibodies. Virology *108*, 381–390. https://doi.org/10.1016/0042-6822(81)90446-3.

62. Giraudon, P., and Wild, T.F. (1981a). Differentiation of measles virus strains and a strain of canine distemper virus by monoclonal antibodies. J. Gen. Virol. *57*, 179–183. https://doi.org/10.1099/0022-1317-57-1-179.

63. ter Meulen, V., Löffler, S., Carter, M.J., and Stephenson, J.R. (1981). Antigenic characterization of measles and SSPE virus haemagglutinin by monoclonal antibodies. J. Gen. Virol. *57*, 357–364. https://doi.org/10.1099/0022-1317-57-2-357.

64. Togashi, T., Orvell, C., Vartdal, F., and Norrby, E. (1981). Production of antibodies against measles virions by use of the mouse hybridoma technique. Arch. Virol. *67*, 149–157. https://doi.org/10.1007/BF01318598.

65. Sheshberadaran, H., Chen, S.N., and Norrby, E. (1983). Monoclonal antibodies against five structural components of measles virus. I. Characterization of antigenic determinants on nine strains of measles virus. Virology *128*, 341–353. https://doi.org/10.1016/0042-6822(83)90261-1.

66. McFarlin, D.E., Bellini, W.J., Mingioli, E.S., Behar, T.N., and Trudgett, A. (1980). Monospecific antibody to the haemagglutinin of measles virus. J. Gen. Virol. *48*, 425–429. https://doi.org/10.1099/0022-1317-48-2-425.

67. Norrby, E., Chen, S.N., Togashi, T., Shesberadaran, H., and Johnson, K.P. (1982). Five measles virus antigens demonstrated by use of mouse hybridoma antibodies in productively infected tissue culture cells. Arch. Virol. *71*, 1–11. https://doi.org/10.1007/BF01315171.

68. Fournier, P., Brons, N.H., Berbers, G.A., Wiesmüller, K.H., Fleckenstein, B.T., Schneider, F., Jung, G., and Muller, C.P. (1997). Antibodies to a new linear site at the topographical or functional interface between the haemagglutinin and fusion proteins protect against measles encephalitis. J. Gen. Virol. *78*, 1295–1302. https://doi.org/10.1099/0022-1317-78-6-1295.

69. Ziegler, D., Fournier, P., Berbers, G.A.H., Steuer, H., Wiesmüller, K.H., Fleckenstein, B., Schneider, F., Jung, G., King, C.C., and Muller, C.P. (1996). Protection against measles virus encephalitis by monoclonal antibodies binding to a cystine loop domain of the H protein mimicked by peptides which are not recognized by maternal antibodies. J. Gen. Virol. *77*, 2479–2489. https://doi.org/10.1099/0022-1317-77-10-2479.

70. Liebert, U.G., Flanagan, S.G., Löffler, S., Baczko, K., ter Meulen, V., and Rima, B.K. (1994). Antigenic determinants of measles virus hemagglutinin

associated with neurovirulence. J. Virol. *68*, 1486–1493. https://doi.org/10.1128/jvi.68.3.1486-1493.1994.

71. Gheuens, J., McFarlin, D.E., Rammohan, K.W., and Bellini, W.J. (1981). Idiotypes and biological activity of murine monoclonal antibodies against the hemagglutinin of measles virus. Infect. Immun. *34*, 200–207. https://doi.org/10.1128/iai.34.1.200-207.1981.

72. Tahara, M., Ohno, S., Sakai, K., Ito, Y., Fukuhara, H., Komase, K., Brindley, M.A., Rota, P.A., Plemper, R.K., Maenaka, K., et al. (2013). The receptor-binding site of the measles virus hemagglutinin protein itself constitutes a conserved neutralizing epitope. J. Virol. *87*, 3583–3586. https://doi.org/10.1128/JVI.03029-12.

73. Hu, A., Sheshberadaran, H., Norrby, E., and Kövamees, J. (1993). Molecular characterization of epitopes on the measles virus hemagglutinin protein. Virology *192*, 351–354. https://doi.org/10.1006/viro.1993.1042.

74. Tahara, M., Bürckert, J.-P., Kanou, K., Maenaka, K., Muller, C.P., and Takeda, M. (2016). Measles virus hemagglutinin protein epitopes: The basis of antigenic stability. Viruses *8*, 216. https://doi.org/10.3390/v8080216.

75. Tahara, M., Ito, Y., Brindley, M.A., Ma, X., He, J., Xu, S., Fukuhara, H., Sakai, K., Komase, K., Rota, P.A., et al. (2013). Functional and structural characterization of neutralizing epitopes of measles virus hemagglutinin protein. J. Virol. *87*, 666–675. https://doi.org/10.1128/JVI.02033-12.

76. Partidos, C.D., and Steward, M.W. (1992). The effects of a flanking sequence on the immune response to a B and a T cell epitope from the fusion protein of measles virus. J. Gen. Virol. *73*, 1987–1994. https://doi.org/10.1099/0022-1317-73-8-1987.

77. Partidos, C.D., Salani, F.B., Ripley, J., and Steward, M.W. (1999). Deconstructing the antigenic profile of a protective epitope from measles virus fusion protein using overlapping peptides. Vaccine *18*, 321–324. https://doi.org/10.1016/S0264-410X(99)00211-X.

78. Obeid, O.E., Partidos, C.D., Howard, C.R., and Steward, M.W. (1995). Protection against morbillivirus-induced encephalitis by immunization with a rationally designed synthetic peptide vaccine containing B- and T-cell epitopes from the fusion protein of measles virus. J. Virol. *69*, 1420–1428. https://doi.org/10.1128/jvi.69.3.1420-1428.1995.

79. Broder, C.C., Xu, K., Nikolov, D.B., Zhu, Z., Dimitrov, D.S., Middleton, D., Pallister, J., Geisbert, T.W., Bossart, K.N., and Wang, L.-F. (2013). A treatment for and vaccine against the deadly Hendra and Nipah viruses. Antivir. Res. *100*, 8–13. https://doi.org/10.1016/j.antiviral.2013.06.012.

80. Tian, D., Battles, M.B., Moin, S.M., Chen, M., Modjarrad, K., Kumar, A., Kanekiyo, M., Graepel, K.W., Taher, N.M., Hotard, A.L., et al. (2017). Structural basis of respiratory syncytial virus subtype-dependent neutralization by an antibody targeting the fusion glycoprotein. Nat. Commun. *8*, 1877. https://doi.org/10.1038/s41467-017-01858-w.

81. Tang, A., Chen, Z., Cox, K.S., Su, H.-P., Callahan, C., Fridman, A., Zhang, L., Patel, S.B., Cejas, P.J., Swoyer, R., et al. (2019). A potent broadly neutralizing human RSV antibody targets conserved site IV of the fusion glycoprotein. Nat. Commun. *10*, 4153. https://doi.org/10.1038/s41467-019-12137-1.

82. Boukhvalova, M.S., Yim, K.C., and Blanco, J. (2018). Cotton rat model for testing vaccines and antivirals against respiratory syncytial virus. Antivir. Chem. Chemother. *26*, 2040206618770518. https://doi.org/10.1177/2040206618770518.

83. Khetsuriani, N., Sanadze, K., Abuladze, M., and Tatishvili, N. (2020). High risk of subacute sclerosing panencephalitis following measles outbreaks in Georgia. Clin. Microbiol. Infect. *26*, 737–742. https://doi.org/10.1016/j.cmi.2019.10.035.

84. Wojtowicz, W.M., Vielmetter, J., Fernandes, R.A., Siepe, D.H., Eastman, C.L., Chisholm, G.B., Cox, S., Klock, H., Anderson, P.W., Rue, S.M., et al. (2020). A human IgSF cell-surface interactome reveals a complex network of protein-protein interactions. Cell *182*, 1027–1043.e17. https://doi.org/10.1016/j.cell.2020.07.025.

85. Takeda, M., Takeuchi, K., Miyajima, N., Kobune, F., Ami, Y., Nagata, N., Suzaki, Y., Nagai, Y., and Tashiro, M. (2000). Recovery of pathogenic measles virus from cloned cDNA. J. Virol. *74*, 6643–6647. https://doi.org/10.1128/JVI.74.14.6643-6647.2000.

86. Pei, J., and Grishin, N.V. (2001). AL2CO: calculation of positional conservation in a protein sequence alignment. Bioinformatics *17*, 700–712. https://doi.org/10.1093/bioinformatics/17.8.700.

87. Ono, N., Tatsuo, H., Hidaka, Y., Aoki, T., Minagawa, H., and Yanagi, Y. (2001). Measles viruses on throat swabs from measles patients use signaling lymphocytic activation molecule (CDw150) but not CD46 as a cellular receptor. J. Virol. *75*, 4399–4401. https://doi.org/10.1128/JVI.75.9.4399-4401.2001.

88. Zyla, D.S., Zipursky, G., Marca, R.D., Lacarbonara, D., Niemeyer, G., Peng, W., Predella, C., Stearns, K., Leedale, C., Miller, J., et al. (2025). Stabilized full-length measles fusion protein elicits potent immunity and protection in vivo. Preprint at bioRxiv, 2025.10.07.681039. https://doi.org/10.1101/2025.10.07.681039.

89. Bovier, F.T., Rybkina, K., Biswas, S., Harder, O., Marcink, T.C., Niewiesk, S., Moscona, A., Alabi, C.A., and Porotto, M. (2021). Inhibition of measles viral fusion is enhanced by targeting multiple domains of the fusion protein. ACS Nano *15*, 12794–12803. https://doi.org/10.1021/acsnano.1c02057.

90. Bloom, N., Ramirez, S.I., Cohn, H., Parikh, U.M., Heaps, A., Sieg, S.F., Greninger, A., Ritz, J., Moser, C., Eron, J.J., et al. (2024). SARS-CoV-2 monoclonal antibody treatment followed by vaccination shifts human memory B-cell Epitope recognition, suggesting antibody feedback. J. Infect. Dis. *230*, 1187–1196. https://doi.org/10.1093/infdis/jiae371.

91. Hastie, K.M., Yu, X., Ana-Sosa-Batiz, F., Zyla, D.S., Harkins, S.S., Hariharan, C., Wasserman, H., Zandonatti, M.A., Miller, R., Maule, E., et al. (2023). Potent Omicron-neutralizing antibodies isolated from a patient vaccinated 6 months before Omicron emergence. Cell Rep. *42*, 112421. https://doi.org/10.1016/j.celrep.2023.112421.

92. Tiller, T., Meffre, E., Yurasov, S., Tsuiji, M., Nussenzweig, M.C., and Wardemann, H. (2008). Efficient generation of monoclonal antibodies from single human B cells by single cell RT-PCR and expression vector cloning. J. Immunol. Methods *329*, 112–124. https://doi.org/10.1016/j.jim.2007.09.017.

93. Giudicelli, V., Brochet, X., and Lefranc, M.-P. (2011). IMGT/V-QUEST: IMGT standardized analysis of the immunoglobulin (IG) and T cell receptor (TR) nucleotide sequences. Cold Spring Harb. Protoc. *2011*, 695–715. https://doi.org/10.1101/pdb.prot5633.

94. Brochet, X., Lefranc, M.-P., and Giudicelli, V. (2008). IMGT/V-QUEST: the highly customized and integrated system for IG and TR standardized V-J and V–D-J sequence analysis. Nucleic Acids Res. *36*, W503–W508. https://doi.org/10.1093/nar/gkn316.

95. Bedinger, D., Parisot, J., and Ditto, N.T. (2025). Competitive Epitope binning using HT-SPR. Methods Mol. Biol. *2937*, 325–360. https://doi.org/10.1007/978-1-0716-4591-8_19.

96. Pfeuffer, J., Püschel, K., Meulen, V.T., Schneider-Schaulies, J., and Niewiesk, S. (2003). Extent of measles virus spread and immune suppression differentiates between wild-type and vaccine strains in the cotton rat model (Sigmodon hispidus). J. Virol. *77*, 150–158. https://doi.org/10.1128/JVI.77.1.150-158.2003.

97. Ackerman, M.E., Moldt, B., Wyatt, R.T., Dugast, A.-S., McAndrew, E., Tsoukas, S., Jost, S., Berger, C.T., Sciaranghella, G., Liu, Q., et al. (2011). A robust, high-throughput assay to determine the phagocytic activity of clinical antibody samples. J. Immunol. Methods *366*, 8–19. https://doi.org/10.1016/j.jim.2010.12.016.

98. Wu, X., Yang, Z.-Y., Li, Y., Hogerkorp, C.-M., Schief, W.R., Seaman, M.S., Zhou, T., Schmidt, S.D., Wu, L., Xu, L., et al. (2010). Rational design of envelope identifies broadly neutralizing human monoclonal antibodies to HIV-1. Science *329*, 856–861. https://doi.org/10.1126/science.1187659.

99. Brown, E.P., Dowell, K.G., Boesch, A.W., Normandin, E., Mahan, A.E., Chu, T., Barouch, D.H., Bailey-Kellogg, C., Alter, G., and Ackerman, M.E. (2017). Multiplexed Fc array for evaluation of antigen-specific antibody effector profiles. J. Immunol. Methods *443*, 33–44. https://doi.org/10.1016/j.jim.2017.01.010.

Please cite this article in press as: Acciani et al., Human neutralizing antibodies targeting the measles virus hemagglutinin and fusion surface proteins, Cell Host & Microbe (2026), https://doi.org/10.1016/j.chom.2026.04.010

STAR★METHODS

KEY RESOURCES TABLE

REAGENT or RESOURCE	SOURCE	IDENTIFIER
Antibodies		
Brilliant Violet 650 anti-human CD20	BioLegend	Cat# 302335, RRID: AB_11218609
R718 anti-human CD19	BD Biosciences	Cat #567343, RRID: AB_2916561
BB515 anti-human CD27	BD Biosciences	Cat# 564642, RRID: AB_2744354
Brilliant Violet 785 anti-human IgD antibody	BioLegend	Cat# 348241, RRID: AB_2629808
PE anti-human CD38 antibody	BioLegend	Cat# 356603, RRID: AB_2561899
APC/Cyanine7 anti-human CD3 antibody	BioLegend	Cat# 344817, RRID: AB_10644011
APC/Cyanine7 anti-human CD14 antibody	BioLegend	Cat# 367107, RRID: AB_2566709
APC/Cyanine7 anti-human CD16 antibody	BioLegend	Cat# 302017, RRID: AB_314217
APC/Cyanine7 anti-human CD56 antibody	BioLegend	Cat# 318332, RRID: AB_10896424
APC/Cyanine7 anti-human CD8a antibody	BioLegend	Cat# 301015, RRID: AB_314133
Anti-human IgG-AF488	Invitrogen	Cat# A11013, RRID: AB_2534080
rat anti-AviTag-AF647 antibody	BioLegend	Cat# 606760, RRID: AB_3068042
goat anti-Human F(ab′)2 AF-488 antibody	Jackson ImmunoResearch	Cat# 109-546-097, RRID: AB_2337849
anti-HIV Env mAb VRC01	NIH AIDS Reagent Program; https://www.hiv.lanl.gov/	Cat# 12033; RRID: AB_2491019
Goat anti-guinea pig C3b antibody, biotin-conjugated	ICL Lab	Cat# GC3-60B-Z, RRID: AB_3740797
Human IgG antibodies against MeV purified using standard methods	This study	N/A
Chimeric mAb-55	Matteo Porotto	N/A
Chimeric mAb-77	Zyla et al.[34]	N/A
Virus strains		
Recombinant MeV-mcherry, genotype B3	Matteo Porotto	N/A
Biological samples		
Human Sera	LJI Clinical Core	N/A
Human PBMCs	LJI Clinical Core	N/A
Chemicals, peptides, and recombinant proteins		
Live/Dead fixable aqua	Thermo Fisher	Cat# L34965
Brilliant stain buffer	BD Biosciences	Cat# 563794
Fetal Bovine Serum	Gibco	Cat# 26140-079
Pen/Strep	Invitrogen	Cat #15140122
Geneticin	Thermo Fisher Scientific	Cat# 10131027
Puromycin	VWR	Cat# mspp-ant-pr-5
cOmplete™, EDTA-free Protease Inhibitor Cocktail	Sigma	Cat# 11873580001
Benzonase Nuclease	Sigma	Cat# 70746-4
NP-40	VWR	Cat# M158-100ML
Ni-NTA Superflow Resin	Qiagen	Cat# 30410
Imidazole	Thermo Fisher Scientific	Cat# O3196-500
Amphipol	Anatrace	Cat# A835
Bio-Beads SM-2 Adsorbent Media	Bio-rad	Cat# 152-3920
Strep-Tactin Superflow Plus resin	Qiagen	Cat# 30004
d-desthiobiotin	Sigma	Cat# D1411-1G

(*Continued on next page*)

Please cite this article in press as: Acciani et al., Human neutralizing antibodies targeting the measles virus hemagglutinin and fusion surface proteins, Cell Host & Microbe (2026), https://doi.org/10.1016/j.chom.2026.04.010

Continued

REAGENT or RESOURCE	SOURCE	IDENTIFIER
Biolock Biotin Binding Solution	IBA	Cat# 2-0205-250
Bis-Tris-Propane	Sigma	Cat# B6755-100G
EZ Link NHS-biotin	Thermo Fisher Scientific	Cat# 20217
succinimidyl ester (NHS)-linked alexa fluor 555 (NHS-AF555)	Thermo Fisher Scientific	Cat# A20009
succinimidyl ester (NHS)-linked alexa fluor 647 (NHS-AF647)	Thermo Fisher Scientific	Cat# A20006
Leucyl leucine methyl ester (LLME)	Cayman Chemical	Cat# 16008
Human FC Block	BD Biosciences	Cat# 564220
Magnetic anti-biotin microbeads	Miltenyi Biotec	Cat# 130-090-485
FluoSpheres NeutrAvidin-Labeled Microspheres	Thermo Fisher	Cat# F8776
magnetic MS columns	Miltenyi Biotec	Cat# 130-042-201
Mitomycin C	Enzo	Cat# BML-GR311-0002
Low IgG FBS	Omega scientific	Cat# FB-06
Insulin	Sigma	Cat# IO516
Transferrin, Human	Sigma	Cat# T8158-100mg
Human rIL-2	GenScript	Cat# Z00368-50
Human rIL-21	Stemcell Technologies	Cat# 78082.1
Iscove's modified Dulbecco's medium	Gibco	Cat# 12440-046
Human rIFN-α 2b	PBL Assay Science	Cat# 11105-1
Human rIL-6	Stemcell Technologies	Cat# 78050.1
Human rIL-15	BioLegend	Cat# 715902
Exonuclease I	Thermo fisher	Cat# EN0582
FastAP™ Thermosensitive Alkaline Phosphatase	Thermo fisher	Cat# EF0652
Platinum SuperFi II Green PCR Master Mix	Invitrogen	Cat# 12369050
Platinum II Hot-Start Green PCR Master mix (2X)	Thermo fisher	Cat# 14001-013
NEBuilder HiFi DNA Assembly master mix	NEB	Cat# E2621L
NEB 5 alpha F'Iq competent E coli	NEB	Cat# C2992I
E-gel96 2% with SYBR safe	Invitrogen	Cat# G720802
Qiaprep 96 Turbo Miniprep kit	Qiagen	Cat# 27191
Goat anti-Human IgG (H&L) Coated Polystyrene Particles	Spherotech	Cat# HUP5-60-5
Praesto AP resin	Purolite	Cat# PR00300-310AP
FIP-HRC MeV F inhibitory peptide	Matteo Porotto	N/A
Uranyl formate	Electron Microscopy Sciences	Cat#22451
Papain	Sigma	Cat#P3125
Paraformaldehyde 16% solution	Electron microscopy sciences	Cat#15710
Hoescht 33342	Thermo/Invitrogen	Cat#H1399
L-cysteine	Calbiochem	Cat#4400
Cell Proliferation and Encoding V/Blue (Tag-it VioletTM) dye	Sartorius	Cat# 97054
Normal goat serum	Thermo Fisher	Cat# PCN5000
Normal rat serum	Stefan Niewiesk	N/A
Yellow-green NeutraAvidin Labeled Microspheres	Invitrogen	Cat# F8776
Neutravidin	Thermo Fisher	Cat# 31000
QUANTI-Luc substrate	Invivogen	Cat# rep-qlc4lg1

(*Continued on next page*)

Please cite this article in press as: Acciani et al., Human neutralizing antibodies targeting the measles virus hemagglutinin and fusion surface proteins, Cell Host & Microbe (2026), https://doi.org/10.1016/j.chom.2026.04.010

Continued

REAGENT or RESOURCE	SOURCE	IDENTIFIER
eBioscience Cell Stimulation Cocktail (500X)	Thermo Fisher	Cat# 00-4970-93
Guinea pig complement serum	Cedarlane	Cat# CL4051
Gelatin veronal buffer	Sigma-Aldrich	Cat# G6514
Streptavidin-R-Phycoerythrin	Millipore Sigma	Cat# 42250
Recombinant DNA		
pCAGGS-MeV H (full-length)-6xhis	This study	N/A
pCG-IgK-MeV H (ectodomain)-TwinStrepII	This study	N/A
pCG-IgK-MeV H (ectodomain)	This study	N/A
pCG-MeV F (full-length)-E170G/E455G-TwinStrepII	Zyla et al.[84]	N/A
pCG-MeV F (ectodomain)-E170G/E455G-TwinStrepII	Zyla et al.[34]	N/A
pCG-MeV F (ectodomain)-E170G/E455GΔfur-TwinStrepII	Zyla et al.[84]	N/A
pMT-MeV F (fectodomain)-E170G/E455G-TwinStrepII	Zyla et al.[34]	N/A
pD649-Hasp-SLAMF1-Fc(DAPA)-AviTag-6xhis	Addgene[85]	Cat# 156642, RRID: Addgene 156642
T7 polymerase	Epoch Life Sciences	GS58929
MeV N protein	Epoch Life Sciences	GS6558900-1
MeV P protein	Epoch Life Sciences	GS59482
MeV L protein	Epoch Life Sciences	GS58944
MeV-mCherry genome, genotype B3	Epoch Life Sciences	GS69677-10
MeV-mCherry genome, H and F genotype D8	Epoch Life Sciences	GS77420-2
MeV-mCherry genome, H and F Schwartz/Moraten vaccine	Epoch Life Sciences	GS77420-1
Commercial Assays		
ExpiFectamine CHO Transfection kit	Thermo Fisher	Cat# A29129
Polyethylenimine HCL Max, MW 40000, Transfection Grade	Polysciences	Cat# 24765-1
Effectene	Qiagen	Cat# 301425
Lipfectamine 2000	Thermo Fisher	Cat# 11668019
1-Step ultra TMB-ELISA	Thermo Fisher	Cat# 34029
PreDictor MabSelect SuRe 20uL 96-well plates	Cytiva	Cat# 28925824
Deposited data		
Negative stain electron microscopy maps of antibodies in complex with MeV H and F ectodomain proteins	Electron Microscopy Data Bank (http://www.emdataresource.org/)	72179 (F + 2B11) 72180 (F + 2D07) 72181 (F + 2G05) 72182 (F + 3A12) 72184 (F + 4F09) 72195 (H + 1C02) 72196 (H + 1C08) 72197 (H + 1G01) 72198 (H + 1G03) 72201 (H + 4D04) 72203 (H + 4D08 and 1C08)
Cryo-EM structures of antibodies in complex with MeV H and F ectodomain proteins	Protein Data Bank (https://www.rcsb.org) / Electron Microscopy Data Bank (http://www.emdataresource.org/)	9Q26/72151 (F + 4F09 and 3A12); 9Q20/72147 (H + 1C08) 9Q24/72149 (H + 1C08 and 4D08) 9Q1Z/72146 (H + 1C02)
Experimental models: Cell lines		
Vero	ATTC	Cat# CCL-81; RRID: CVCL_0059
HEK293F	Thermo Fisher Scientific	Cat# R79007
ExpiCho-S cells	Thermo Fisher Scientific	Cat# A29127; RRID: CVCL_5J31
Drosophila: Schneider 2	ThermoFisher Scientific	Cat# R69007; RRID: CVCL_Z232

(*Continued on next page*)

Please cite this article in press as: Acciani et al., Human neutralizing antibodies targeting the measles virus hemagglutinin and fusion surface proteins, Cell Host & Microbe (2026), https://doi.org/10.1016/j.chom.2026.04.010

Continued

REAGENT or RESOURCE	SOURCE	IDENTIFIER
HEK 293T	ATCC	CRL-3216
Vero-SLAMF1	Ono et al.[86]	N/A
THP-1	ATCC	Cat# TIB-202; RRID: CVCL_0006
Jurkat-Lucia NFAT CD16 cells	Invivogen	Cat code jktl-nfat-cd16
Experimental models: Organisms/strains		
Sigmodon hispidus, cotton rat strain	Envigo, Inc.	N/A
Software and algorithms		
International ImMunoGeneTics Informations System (IMGT)/V-Que	N/A	imgt.org
GraphPad Prism 10	GraphPad Software	https://www.graphpad.com/
Carterra "Kinetics" and "Epitope" software packages	Carterra	https://wwww.carterra-biocom/
CryoSPARC	CryoSPARC	www.cryosparc.com
Chimera X	Pettersen et al.[54]	N/A
SWISS-MODEL	Waterhouse et al.[56]	N/A
PHENIX	Adams et al.[57]	N/A
COOT	Emsley et al.[58]	N/A
PISA	EMBL-EBI[61]	N/A
BioTek Gen5 3.11	Agilent	N/A
Other		
OptoSeq® BCR Kit v2	Bruker Cellular Analysis	Cat# 750-08238
Bruker Cell Analysis Beacon Optofluidic System	Bruker Cellular Analysis	https://brukercellularanalysis.com
OptoSelect 11K chip & wetting solution	Bruker Cellular Analysis	Cat# 750-08090
Tecan Spark 10M plate reader	Tecan	www.tecan.com
Carterra LSA	Carterra	https://carterra-bio.com/lsa/
HC30M LSA chip	Carterra	Cat# 4279
FACSSymphony S6 cell sorter	BD Biosciences	www.bdbiosciences.com
Countess II FL automated cell counter	Thermo Fisher Scientific	www.thermofisher.com
Superdex 200 pg HiLoad 16/600 column	Cytiva	Cat# 28989335
StrepTrap HP column	Cytiva	Cat# 28-9075-47
Resource Q anion exchange chromatography column	Cytiva	Cat# 17117901
Superdex 200 Increase 10/300 GL column	Cytiva	Cat# 28990944
HiPrep 26/10 desalting column	Cytiva	Cat# 17508701
PD G-25 miditrap	Cytiva	Cat# 28918008
HiTrap Fibro PrismA column	Cytiva	Cat# 17549855
CellInsight CX5 HCS Platform	Thermo Fisher Scientific	www.thermofisher.com
BioTek Cytation 5 Cell Imaging Multimode Reader	Agilent	www.agilent.com
Titan Halo electron microscope	Thermo Fisher Scientific	www.thermofisher.com
Titan Krios electron microscope	Thermo Fisher Scientific	www.thermofisher.com
CF400-Cu grids	Electron Microscopy Sciences	Cat# CF400-Cu
IQue3 HTS cytometer	Sartorius	www.sartorius.com
Prometheus Panta	NanoTemper	www.nanotempertech.com
FlexMap 3D reader	Luminex	N/A

Please cite this article in press as: Acciani et al., Human neutralizing antibodies targeting the measles virus hemagglutinin and fusion surface proteins, Cell Host & Microbe (2026), https://doi.org/10.1016/j.chom.2026.04.010

EXPERIMENTAL MODEL AND STUDY PARTICIPANT DETAILS

Human sample donation

The La Jolla Institute for Immunology (LJI) Clinical Core recruited healthy adults for pre- and post- SARS-CoV-2 vaccination blood donations and collected blood draws under IR-B approved protocols (IB-233-0820 A3). All donors gave informed consent at the time of study enrollment and provided information on gender, ethnicity, age, and MMR vaccination history (including a date approximation). Vaccinated subjects did not report exposure to authentic measles virus, although we cannot rule out unknown, subclinical infections. Pre-SARS-CoV-2 vaccine serum and PBMC samples were used in this study. Samples were coded, and then de-identified prior to analysis.

Plasmids

We used full-length Measles virus (MeV) hemagglutinin (H) and fusion (F) constructs for donor serum IgG screens, and ectodomain constructs for all downstream experiments and analyses. Constructs encoded MeV H (Uniprot Q786F2) and F (Uniprot Q786F3) reference sequences from strain IC323 (derived from the highly virulent wild type Ichinose-B95a strain rescued in B95a cells).[85] Full-length MeV H was codon optimized, synthesized, and sub-cloned into the mammalian expression vector pCAGGS[34] (Epochlifescience) with a C-terminal 6x histidine tag. The H ectodomain (H_{ECT}, residues 149-617) was subcloned to a pCG vector using the NEB High Fidelity Phusion polymerase and Gibson Assembly Master Mix (NEB). The pCG_H_{ECT} gene was flanked by a 5' Ig Kappa leader sequence and a C-terminal twin StrepII tag. We also cloned an untagged version of pCG-H_{ECT} for structural studies. The full-length MeV fusion protein (F) and ectodomain (F_{ECT}, residues 1-494) from MeV strain Ichinose-B95a were cloned into pMT-puro or pCG expression vectors. All F constructs contained two ("2M": E170G and E455G) or three ("3M": 2M + Δfurin cleavage site) stabilizing mutations, which maintain F in the prefusion conformation, and a C-terminal twin Strep-TagII. The pMT-puro plasmid encoding F_{ECT} 2M was synthesized as previously described.[34] For receptor-mAb competition assays we used a pD649-Hasp-SLAMF1-Fc(DAPA)-AviTag-6xhis plasmid[84] (a gift from Chris Garcia; Addgene plasmid #156642; http://n2t.net/addgene:156642; RRID:Addgene_156642), which encodes the extracellular Ig-like V and C2 domains of SLAMF1 fused to human FC (SLAMF1-huFC).

Cell lines

Vero (African green monkey kidney), Vero-SLAMF1 cells (Vero cells stably expressing MeV receptor human SLAMF1),[87] and HEK293T cells were grown in Dulbecco's modified Eagle's medium (DMEM; Life Technologies; Thermo Fisher Scientific) supplemented with 10% (vol/vol) fetal bovine serum (FBS, Life Technologies; Thermo Fisher Scientific) and 1% penicillin-streptomycin (pen/strep, 100 U/mL penicillin and 100 μg/mL streptomycin) at 37°C and 5% CO_2. Vero-SLAMF1 cell culture medium also included 1 mg/ml geneticin (Thermo Fisher Scientific). ExpiCHO cells were maintained in ExpiCHO Expression Medium (Gibco) supplemented with 8 mM L-glutamine in a humidified incubator at 37°C with 8% CO_2. HEK 293F cells were maintained in FreeStyle293 Expression Medium (Gibco) at 37°C with 5% CO_2. *Drosophila* S2 cells were cultured at 25°C (no CO_2) in complete Schneider's *Drosophila* Medium (Gibco) with 10% heat-inactivated FBS and 1% pen/strep or in serum-free Insect Xpress Medium (Lonza). The human monocytic cell line, THP-1, was purchased from ATCC and maintained in RPMI-1640 supplemented with 10% FBS and 55μM beta-mercaptoethanol at 37°C with 5% CO_2. Jurkat-Lucia NFAT CD16 cells (Invivogen) were cultured in RPMI-1640 supplemented with 10% FBS, 1 mM sodium pyruvate, 1x non-essential amino acids, 1x pen/strep, 100 μg/mL Normocin, 100 μg/mL Zeocin, and 10 μg/mL Blasticidin.

METHOD DETAILS

MeV antigen and receptor production and purification

Full-length H purification via 6x his tag

HEK293F cells were expanded to a density of approximately 1 x 10^6 cells/mL in at least 500 mL media on the day of transfection. Transfection was performed using 1μg/mL pCAGGS-H-F_{FL}-6xhis[88] and polyethylenimine (PEI, Polysciences) at a ratio of 1:3 DNA:PEI. The cells were cultured for five days, then centrifuged at 4000 x g and 10°C. The cell pellet was resuspended in a volume equivalent to one-tenth of the initial culture (50 mL) in ice-cold HBS buffer (50 mM HEPES, pH 8.0, 150 mM NaCl). Protease inhibitor cocktail (200 μL) and 1.5 μL of Benzonase were added to the suspension, and the mixture was kept on ice. The suspension was then homogenized gently via a douncer. NP-40 (ThermoFisher) was added to the homogenized cells at a final concentration of 2%. The cells were incubated at 4°C for 2 h with gentle rocking at approximately 1 Hz. The solubilized solution was centrifugated at 38,000 x g for 30 min at 4°C. The supernatant was incubated overnight with 1 mL of equilibrated NiNTA beads (Qiagen) at 4°C with rocking. This mixture was then diluted with HBS to reduce the final NP-40 concentration. The resin was washed with 0.06% NP-40 HBS, 0.06% NP-40 HBS with 20 mM imidazole (Fisher Scientific), then 0.06% NP-40 HBS with 50 mM imidazole, followed by elution with 0.06% NP-40 HBS 250 mM imidazole. The eluted medium was mixed with amphipol (Anatrace) (5 mg amphipol to 1 mg protein) for 20 to 30 min, then mixed with Bio-Beads (Bio-rad) to remove NP-40. Biobeads were removed using gravity filtration and the imidazole was removed by applying the filtered medium to a Hiload 16/600 superdex column (Cytiva) equilibrated with HBS buffer on an ÄKTA Pure system. Purified protein was flash-frozen in liquid nitrogen. Protein concentration was estimated using the molar extinction coefficient at 280 nm (97,750 M-1 cm-1).

Please cite this article in press as: Acciani et al., Human neutralizing antibodies targeting the measles virus hemagglutinin and fusion surface proteins, Cell Host & Microbe (2026), https://doi.org/10.1016/j.chom.2026.04.010

Full-length F purification via Twin StrepII tag

Expression of full-length MeV-F in HEK293F cells and supernatant harvesting was performed as mentioned above using the pCG-F-FL-2M plasmid.[88] Supernatant from homogenized cells was incubated overnight with 1 mL of equilibrated Streptactin resin (Qiagen) at 4°C with rocking. This mixture was then diluted with HBSE (50 mM HEPES ph8, 150 mM NaCl, 1mM EDTA) to reduce the final NP-40 concentration, then washed with 10 mL HBSE containing 0.06% NP-40. Amphipol was added to the resin and incubated for 2 h at 4°C with rocking. The resin was then washed three times with 2 mL HBSE, and protein was eluted with HBSE containing 5 mM d-desthiobiotin. Purified protein was flash-frozen in liquid nitrogen. Protein concentration was estimated using the molar extinction coefficient at 280 nm (57,700 M-1 cm-1).

H ectodomain purification via Twin StrepII tag

ExpiCHO cells were transiently transfected with plasmid encoding the H ectodomain construct (pCG_IgK_H_{ECT}_TwinStrep) using the ExpiFectamine CHO Transfection Kit (Gibco) in accordance with the manufacturer's "high titer" protocol. Following expression, cells were removed by centrifugation at 4,000 × g for 15 min. The clarified supernatant was incubated with 300 μL Biolock (IBA GmbH) and the pH was adjusted to 8.0 with 1 M HEPES (final concentration 50 mM). After 30 min, the medium was further clarified by centrifugation at 4,000 × g for 10 min and sterile-filtered using a 0.22 μm filter. The filtered medium was applied to a Strep-Tactin HP column (Cytiva) equilibrated with HBS buffer (20 mM HEPES, pH 8.0, 150 mM NaCl) on an ÄKTA Pure system. After extensive washing with HBS buffer to remove nonspecifically bound proteins, tagged H_{ECT} was eluted using 5 mM desthiobiotin (Sigma) in HBS. Fractions containing the protein of interest were pooled, concentrated to 0.8 mg/mL, and flash-frozen in liquid nitrogen. Protein concentration was estimated using the molar extinction coefficient at 280 nm (84,800 M-1 cm-1).

H ectodomain purification via ion exchange

Due to potential conformational constraints imposed by the twin-strep tag in close proximity to the stalk region, an untagged H_{ECT} variant was also expressed and purified. Following removal of cells by centrifugation, the supernatant was adjusted to pH 9.0 using 1 M Bis-Tris-Propane (Sigma) based on the calculated isoelectric point (pI ≈ 6.6) for H_{ECT}. The medium was filtered through a 0.22 μm membrane and loaded onto a 6 mL Resource Q anion exchange column (Cytiva). Protein was eluted using a 10-column volume linear gradient up to 100% of elution buffer. Eluted fractions containing H_{ECT} were concentrated and subjected to size-exclusion chromatography using a Superdex 200 Increase 10/300 GL column (Cytiva). Fractions corresponding to the H_{ECT} peak were pooled, concentrated to ~0.4 mg/ml, and flash-frozen.

F ectodomain purification via Twin StrepII tag

F ectodomain was produced in Drosophila S2 cells as previously described.[34] To summarize, cells were seeded in a six-well plate in complete Schneider's medium, then transfected with a F ectodomain plasmid the following day using the Effectene (Qiagen) transfection protocol. Cells were transferred to a T25 flask and cultured with puromycin (6 μg/ml) on day 5, then expanded to a T75 flask and cultured with Insect Cell Expression Culture Media (Lonza) with 6 μg/ml puromycin. Cells were expanded to 2 L shaking flasks, induced with 500 μM $CuSO_4$ at 1 × 10^7 cells/mL, and harvested four days after induction. Cells cleared via centrifugation at 5000 x *g* for 20 min. The supernatant was adjusted to pH 8.0 with 1 M HEPES, and incubated with Biolock (IBA) and NaCl (final concentration 800 mM). The supernatant was loaded onto a pre-washed StrepTrap HP 5 mL column (Cytiva). Purified F ectodomain protein was eluted with high-salt HBS (20mM HEPES, 800 mM NaCl) containing 5 mM d-desthiobiotin. The purified protein buffer was exchanged for high-salt HBS-only buffer using a HiPrep 26/10 desalting column (Cytiva). Purified protein was flash-frozen in liquid nitrogen. Protein concentration was estimated using the molar extinction coefficient at 280 nm (48,820 M-1 cm-1).

H_{ECT} and F_{ECT} labeling

We used biotinylated or fluorescently-labeled H/F constructs for antigen-specific memory B cell enrichment, antigen-specific PBMC quantification via flow cytometry, and single-cell memory B cell identification on the Bruker Cell Analysis Beacon. Non-specific biotinylations were performed using EZ Link NHS-biotin (20217, Thermo Scientific) according to the manufacturers protocol. Proteins were incubated with NHS-biotin for 2 h at 4°C while gently shaking. Reactions were quenched with 50uL Tris HCl (1M, pH 8) for 10 min. For fluorescent detection, proteins were labeled with succinimidyl ester (NHS)-linked alexa fluor 555 (NHS-AF555, A20009, Thermo Fisher Scientific) or Alexa Fluor 647 (NHS-AF647, A20006, Thermo Fisher Scientific) according to the manufacturer's protocol. Proteins were labeled in 0.1M sodium bicarbonate at 4°C with periodic vortexing. Biotinylated and fluorescent proteins were desalted using PD G-25 miditraps (Cytiva, 28918008) into HBS, then aliquoted, flash-frozen in liquid nitrogen, and stored at -80°C. Protein concentration was estimated using the molar extinction coefficient at 280 nm (84,800 M-1 cm-1 for H_{ECT}, 48,820 M-1 cm-1 for F_{ECT}).

SLAMF1-huFC purification

A 50 mL culture of ExpiCHO cells was transfected with pD649-SLAMF1-huFC plasmid using the ExpiFectamine CHO Transfection Kit (Gibco) in accordance with the manufacturer's "max titer" protocol, and supernatant was harvested after 10 days. Cells were removed by centrifugation at 4,000 × g for 15 min. Supernatant pH was adjusted to pH 7.5 using 1M tris-hydrochloride (pH 7.5). SLAMF1-huFC was purified from supernatant using Praesto AP resin (Purolite PR00300-310AP), then dialyzed into PBS and stored at -80°C.

Virus

Recombinant Measles virus strains rMeV-B3, rMeV-D8, or rMeV-Schwartz, each encoding the mCherry reporter gene (MeV-mcherry), were obtained via viral rescue. Briefly, HEK293T cells were transfected using Lipofectamine 2000 with cDNA constructs encoding the T7 polymerase (GS58929), MeV-mCherry B3 genome (GS69677-10, with mCherry), and measles proteins N

(GS6558900-1), P (GS59482), and L (GS58944) (MeV proteins sourced by Epoch Life Sciences). For rMeV-D8 and rMeV-Schwartz, the B3 genome H and F genes were replaced with con H and F from genotype D8 (GS77420-2) or the Schwartz/Moraten vaccine strain (GS77420-1)(Epoch Life Sciences). Cells were incubated overnight at 37°C in Opti-MEM medium, then the medium was replaced with DMEM 10% FBS and pen/strep ("complete" DMEM, or cDMEM). Cells were heat-shocked by incubation in a 42°C water bath for 3 h, then returned to 37°C for 48 h. Next, transfected HEK293T cells were detached and overlaid with Vero-SLAMF1 cells in T-75 flasks to facilitate rescued virus amplification. The virus underwent four passages and was titrated to a concentration of 10^6 plaque-forming units per milliliter (PFU/ml). RNA from the virus sample was then sequenced and the virus stock used for subsequent *in vivo* experiments.

For virus stock propagation, Vero-SLAMF1 cells were infected with 0.05 to 0.01 PFU/mL at 32°C in cDMEM. When extensive cell-cell fusion was observed, the media was replaced with fresh cDMEM, and cells were scraped into the new media. Cells were freeze-thawed at -80°C and 25°C twice to release cell-associated virus particles, then spun at 3000 to 4000 RPM. Media was replaced, and the resuspended cell pellet was aliquoted, and stored at -80°C.

Virus stock titers were determined using end-point dilutions and fluorescent cell quantification via the CellInsight CX5 HCS Platform (Thermo Fisher). Because cells infected with MeV form large multi-nucleated syncytia, automated cell quantification was simplified by treating infected cells with 500nM FIP-HRC, a F-specific peptide that inhibits MeV cell-cell spread and syncytia formation.[89]

Serum ELISAs

Donor serum samples were heat-inactivated for 30 min at 55°C. Half-area high-binding 96 well plates were coated overnight with 200 ng/well of purified full-length MeV H and F at 4°C. Wells were blocked with 3% milk in PBS for 3 h, followed by incubation with donor sera diluted 1:100, 1:1000, 1:10,000, and 1:100,000 in PBS with 0.05% Tween-20 (PBS-T) and 1% milk for 1 h. Plates were washed five times with PBS-T, then incubated with goat anti-human IgG-HRP (Invitrogen 31413), diluted 1:7500 in 1% milk PBST for 1 h. Plates were washed five times with PBS-T, then developed using 1-Step Ultra TMB-ELISA substrate (Thermo Fisher 34029). Reactions were stopped with 1M H_2SO_4, and plate signals at 450 nm were measured using a Tecan Spark 10M plate reader. Donor serum reactivities to MeV H and F individually and summed are displayed as heatmaps (red = higher reactivity, beige = lower reactivity).

MeV memory B cell detection via flow cytometry

Cryopreserved PBMCs from donors #3920, #0003, and #4168 were prepared and stained as previously described,[90] with some modifications as follows: PBMCs were thawed at 37°C and then resuspended in prewarmed cDMEM with Benzonase (Sigma 70746-4). Cell counts and viability after washing were assessed on a Countess II FL (Invitrogen). PBMCs were placed in U-bottom 96-well plates and stained with 200 ng H_{ECT}-AF647 or F_{ECT}-AF647 in Brilliant Stain Buffer (BSB, BD Biosciences cat#563794) for 1 h at 4°C, protected from light. Cells were then washed in BSB and resuspended in a staining cocktail containing surface antibodies diluted in BSB for 30 min at 4°C in the dark. Viability staining was performed using LIVE/DEAD fixable aqua dead cell stain (Thermo cat#L34965), and cells were incubated at 4°C for 30 min. Cells were washed twice in PBS and resuspended in FACS sort buffer (0.5 M EDTA, 25 mM HEPES pH 8, 1% FBS, in Hank's balanced salt solution [Thermo Fisher, cat#14175095]). The acquisition was performed using a FACSSymphony S6 cell sorter. The frequency of antigen-specific PMBCs was expressed as a percentage of total memory B cells (Live, Lymphocytes, Singlets, $CD3^-$ $CD14^-$ $CD16^-$ $CD56^-CD8a^-$, $CD19^+$ $CD20^+$, $CD20^+$ $CD38^{int/-}$, IgD^- and/or $CD27^+$).

mAb identification and production

MemB enrichment

Cryopreserved PBMCs were thawed and washed twice in DMEM 20% FBS and Benzonase (50 U/mL) via centrifugation (500g for 10 min). Cells were resuspended in DMEM 20% FBS and assessed for density and viability, filtered through mesh, pelleted, and resuspended in cold PBS (0.5% BSA, 2mM EDTA, pH ~7.3). Cells were mixed with biotinylated H_{ECT} and F_{ECT} (2 ng/uL) for 30 min at 4°C, then washed and blocked with Human Fc block (BD #564220) for 15 min at 4°C. Magnetic anti-biotin microbeads (Miltenyi Biotec #130-090-485) were then added to cells for 15 min at 4°C. Cells were washed and resuspended in PBS (0.5% BSA, 2mM EDTA, pH ~7.3), then passed through magnetic MS columns (Miltenyi Biotec 130-042-201). Antigen-specific PBMCs bound to antigen-coated anti-biotin beads were eluted from the column. We performed two parallel PBMC enrichments, one with biotinylated H_{ECT} and F_{ECT} combined, and one with biotinylated F_{ECT} alone, as we previously observed the ability for H_{ECT} to bind to and introduce non-target toxic lymphocytes to our enriched cell populations. To mitigate this lymphocyte introduction, pre-H+F-enriched cells were first treated with 1 mM L-Leucyl-L-Leucine methyl ester (LLME, Cayman Chemicals 16008) to eliminate cytotoxic cells.

MemB activation and Beacon analysis

H_{ECT}- and F_{ECT}- enriched cells were activated and loaded onto a Bruker Cellular Analysis Beacon for single-cell identification as previously described.[91] Enriched cells were overlaid on feeder mitomycin-treated MS40L cells in 6-well plates in complete Iscove's medium (cIMEM, 20% Low IgG FBS, 1% pen/strep, 5 μg/mL insulin, and 50 μg/mL human transferrin) supplemented with 100 U/ml Hu rIL-2 (GenScript), and 100 ng/mL Hu rIL-21 (Stemcell Technologies). Seven days later, cell densities were readjusted to 250,000 cells/mL and culture media was changed to cIMEM supplemented with 500 U/mL Hu rIFN-α 2b (PBL Assay), 50 ng/mL Hu rIL-6 (Stemcell Technologies) and 10 ng/mL Hu rIL-15 (BioLegend). Three days later (10 days after enrichment), cells were loaded onto OptoSelect 11K chips (Bruker Cellular Analysis), wherein they were isolated as single cells in nanoliter pens using OEP light cages. Antigen-specific antibodies were detected in a 30-min time course assay using anti-human IgG beads (Spherotech cat#HUP5-60-5) that were

Please cite this article in press as: Acciani et al., Human neutralizing antibodies targeting the measles virus hemagglutinin and fusion surface proteins, Cell Host & Microbe (2026), https://doi.org/10.1016/j.chom.2026.04.010

resuspended in media containing H_{ECT}-AF555 (6 μg/mL), F_{ECT}-AF647 (6 μg/mL) and goat anti-human IgG-AF488 (1 μg/mL, invitrogen cat# A11013).

mAb cloning

Cellular RNA to cDNA synthesis was performed on-chip using the Bruker OptoSeq BCR kit, according to the manufacturer's instructions and previously described.[91] Total cDNA was amplified using the Platinum SuperFiII polymerase (Invitrogen), and cleaned up enzymatically. Antibody heavy chain (HC) and light chain (LC) variable domains were amplified with one or two rounds of nested PCR using the PlatinumII Hot-Start polymerase (Invitrogen) and previously published primer sets.[92] PCR products were assessed using 96-well E-gels (ThermoFisher), and paired wells were sequenced and analyzed using the International ImMunoGeneTics Informations System (IMGT)/V-Que.[93,94] Unique variable heavy (VH) and variable light (VL) domains were cloned into linearized antibody expression vectors (human IgG1 and relevant light chain) using Gibson Assembly (NEB) according to the manufacturer's protocol. Ligation reactions were transformed into 5-alphaF'Iq competent *E. coli* cells (NEB). QIAprep 96 Turbo Miniprep Kits (Qiagen 27191) were used to purify plasmids. Plasmids were sequenced to ensure that genes were in-frame, and the cloned VH and VL domains were compared to PCR sequences.

mAb and Fab production and purification

Test expressions of each mAb were carried out in 2.5 mL cultures of ExpiCHO cells cultured in 24-well blocks. Cells were transiently transfected and incubated at 37°C, 5% CO_2 for five days. Supernatants were clarified and either 1) used directly in preliminary kinetics and neutralization screens (Figure S1) or 2) applied to PreDictor MabSelect SuRe 20uL 96-well plates (Cytiva Cat# 28925824) to isolate mAbs. Purified mAbs were used for H_{ECT} and F_{ECT} epitope binning to further select mAbs of interest. A panel of sixteen mAbs was produced in larger (25-100 mL) expiCHO cell cultures and purified from cell supernatants using Praesto AP resin (Purolite PR00300-310AP) or a HiTRap Fibro PrismA column (Cytiva). MAbs were then dialyzed into PBS and stored at -20°C.

For structural analyses, purified mAbs were digested into antibody fragments (Fabs) by incubating antibodies with papain (2.5 mg/mL) in the presence of 10mM L-cysteine for 3 h at 37°C. Digestions were stopped by adding iodoacetamide (50mM). Fabs were separated from Fc fragments using Praesto AP resin, then dialyzed into PBS and stored at -20°C. mAb and Fab concentrations were determined using the absorbance at 280nM and the general IgG extinction coefficient 210,000M^{-1} cm^{-1}.

High-throughput SPR binding kinetics

Binding kinetics measurements were performed on the Carterra Lodestar Array (LSA) platform using HC30M sensor chips (Carterra) at 25°C. Two microfluidic modules, a 96-channel print-head (96PH) and a single flow cell (SFC), were used to deliver samples onto the sensor chip. Sensor chips surfaces were conditioned using 25 mM MES pH 5.5 with 150 mM NaCl and 0.05% Tween 20 and activated with a freshly prepared solution of 130 mM 1-ethyl-3-(3-dimethylaminopropyl)carbodiimide hydrochloride (EDC) + 33 mM N-hydroxysulfosuccinimide (Sulfo-NHS) in 0.1 M MES pH 5.5 using the SFC. MeV mAbs were either captured from cell supernatant on to chips using goat anti-Human IgG Fc secondary antibody (50ug/mL, VWR, 103255–066) or purified, diluted to 5 (MeV-H mAbs) or 2.5 μg/mL (MeV-F mAbs) in 10 mM NaOAc (pH 4.5, 0.05% Tween 20), and directly immobilized on to chip surfaces for 20 min. All IgG immobilization steps were followed by a 7-min injection of 1 Methanolamine-HCl (pH 8.5) using the SFC to quench unreactive esters.

A seven-fold dilution series of MeV-H_{ECT} or -F_{ECT} was prepared in 1xHBSTE-BSA (10 mM HEPES pH 7.4, 150 mM NaCl, 3 mM EDTA and 0.01% Tween 20) buffer. Each antigen was then injected onto the chip surface using the SFC, from the lowest to the highest concentration, without regeneration in between, using 1xHBSTE-BSA running buffer. Five to six injections of buffer before the lowest non-zero concentration were used for signal stabilization. For each concentration, baseline data were collected for 120 s, association data for 300 s and dissociation data for 900 s. After the titration of each analyte, the chip surface was regenerated with two pulses (20-30 s per pulse) of 10 mM Glycine, pH 2.0.

Titration data were processed with the Kinetics software package (Carterra), including reference subtraction, buffer subtraction and data smoothing. H_{ECT} or F_{ECT} binding time courses for each antibody were fitted to a 1:1 Langmuir model to derive K_a, K_d and K_D values.

High-throughput SPR epitope binning

Premix epitope binning was performed on the Carterra Lodestar Array (LSA) platform using HC30M sensor chips (Carterra) at 25°C in 1xHBSTE-BSA running buffer.[95] The chip was activated as described above. Each mAb was immobilized on the chip's surface and separately mixed with H_{ECT} or F_{ECT} at a 4x molar excess of IgG to antigen in 1xHBSTE-BSA. MAb-antigen solutions were injected over the chip's surface for 5 min. Chip surfaces were regenerated after every cycle using single pulses (30 s) of 10 mM Glycine, pH 2.0. Data was processed and analyzed with Epitope software (Carterra).[95] Briefly, data was referenced using unprinted locations on the array. The binding level of the analyte antibody-antigen complex was compared to that of an antigen-alone injection. Signals that were significantly increased relative to the antigen-alone controls are described as sandwiches and represent non-blocking behavior. Competition results were visualized as a heatmap that depicts blocking relationships of analyte/ligand pairs. Antibodies with similar patterns of competition are clustered together in a dendrogram and are assigned to shared communities.

Epitope mapping using NS-EM

Fab-antigen complex formation, grid preparation, NS-EM, and 3D volume reconstruction

MeV H_{ECT} or F_{ECT} were incubated with an excess of Fabs for 15-30 min at RT and applied to freshly glow-discharged, carbon-coated 400 mesh copper grids (C-flat, Electron Microscopy Sciences). Following a rapid water wash, grids were stained with 1% uranyl

acetate for 1 min. Excess stain was removed and grids were air dried. TEM images were collected using SerialEM on a Titan Halo 300kV electron microscope using a Gatan K3 direct electron detector. Motion correction, CTF estimation, particle picking, 2D classification and 3D reconstruction were performed using cryoSPARC software algorithms. Reconstructions were evaluated using Gold Standard Fourier Shell Correlation (GSFSC) metrics to prevent overfitting and determine the final map resolution at an FSC value of 0.143.

Fab-antigen complex modeling

Fab-antigen complexes were modeled by rigid-body fitting of individual H_{ECT}, F_{ECT} and Fab models into cryoSPARC densities in ChimeraX. Atomic H_{ECT} and Fab models were generated using AlphaFold2 and AlphaFold3 predictions. N-linked glycans ($Man_5GlcNAc_2$) were modeled on H_{ECT} residues N200, N215, and N416 using Alphafold3.[8,38] The cryo-EM structure of F_{ECT}2M (PDB ID: 8UUP) was used as a starting model.[34] Density handedness was determined via visual inspection of docked antigen models.

Fab-antigen epitope mapping

We generated 3D molecular map surfaces (molmaps) from the docked H_{ECT} or F_{ECT} atomic models at 16 Å using ChimeraX command (molmap #model 16 gridspacing 2) and rendered rough representations of Fab interfaces by coloring regions of these surfaces that fell within 12 Å of docked Fabs.

AlphaFold3 modeling of antibody-antigen complexes

We generated antibody-antigen complex predictions for both the H and F glycoproteins in order to evaluate whether AlphaFold3 multimer modeling could accurately predict experimental NS and cryo-EM observations and support interface identification in the absence of high-resolution structural data. For the F glycoprotein, the ectodomain (residues 24–495) was modeled as a single continuous chain and replicated three times to model the trimeric complex. Similarly, two copies of the H ectodomain (residues 149–617) were used to model its dimeric architecture. Each antibody was modeled in complex using the variable regions (VH and VL) of the heavy and light chains as input. Predictions were generated using the AlphaFold3 multimer framework.

To account for glycosylation, AlphaFold3-generated JSON files were generated using the UniProt2AlphaFold3 software (https://github.com/dzyla/AF3_JSON_generator), which annotated sequences with experimentally determined glycosylation sites annotated in the Uniprot database. Predicted models (five per antibody-antigen pair) were aligned and assessed for convergence of antibody binding sites (precision) and their agreement with experimental data (accuracy) using root-mean-square deviation (RMSD) analyses

Accuracy and precision RMSD values (A-RMSD/P-RMSD) were calculated by first defining centroids- or the XYZ coordinates- of each predicted and experimental Fab complex model in ChimeraX. For A-RMSDs, we then quantified the average Euclidean distance from model centroids to the experimental centroid. For P-RMSDs, we quantified the average Euclidean distance from model centroids to a theoretical "centroid of centroids" coordinate, which reflects the spatial spread of the centroids around their collective center. Because the typical resolution achievable using NS-EM is approximately 20Å, we considered predicted models sets to be accurate/precise if the overall A-RMSD and P-RMSD values for each antigen-mAb set were below 20Å.

In vitro viral neutralization of rMeV-B3-mcherry

Confluent Vero-SLAMF1 cells were diluted 1:20 and seeded in 96-well plates (100 uL/well). The next day, mAbs and virus were combined and applied to cells for infection. MAbs were serially diluted 1:5 (final concentration range $2.56x10^{-4}$ to 20 ug/mL) and pre-incubated with $5x10^3$ FFU/mL rMeV-B3-mCherry for 1 h at room temperature (RT). Vero-SLAMF1 supernatants were removed, and mAb-virus mixtures were added to cells and incubated at 37C 5% CO2 for three h. Because adherent cell lines infected with MeV fuse together to form giant multi-nucleated syncytia that are difficult for standard fluorescent detectors to define and quantify, we treated infected cells with FIP-HRC, a F-specific peptide that inhibits MeV cell-cell spread and syncytia formation.[89] After 3 h, cell infection media was replaced with media containing 500 nM FIP-HRC. Cells were then returned to the incubator for infections to proceed overnight. The next day, cells were fixed and stained using 3.7% formalin in PBS containing Hoescht (1:1000) for 10 min at RT.

In vitro viral neutralization of MeV genotypes B3, D8, and the Schwartz vaccine strain

Vero-SLAMF1 cells were plated in 96-well plates (1×10^4 cells/well). The following day, cells were treated with serial dilutions of the indicated antibodies (0.05 to 100 nM). Cells were then infected with the MeV-mCherry B3 expressing H and F from genotype B3, D8, or the Schwartz vaccine (derived from genotype A) for 3 h at 37°C (200-300 pfu/well). After 3h, the medium was replaced with medium containing 2% of methylcellulose 2× complete medium (1:1). After 48 h, infected fluorescent cells were quantified.

In vivo mAb prophylactic and therapeutic protection in cotton rats

Inbred cotton rats (*Sigmodon hispidus*, cotton rat strain "Hsd:Cotton Rat" without genetic modifications) were purchased from Envigo, Inc., Indianapolis. Male and female cotton rats aged 4 to 10 weeks were used for experiments. Isoflurane-anesthetized rats were injected intraperitoneally with each mAb (1mg/kg, 5 animals per mAb), PBS (3-4 animals), or human IgG (5 animals) purified from pooled sera (20mg/kg, Carimune, CSL Behring, NT titer 640) 14 h before infection, or 24 or 48 h after infection. Anesthetized rats were then inoculated intranasally with 100 µl $2x10^5$ $TCID_{50}$ MeV B3-GFP. Four days after infection (when animals typically reach peak MeV titer in the lung tissue,[96] animals were euthanized by CO_2 inhalation, and their lungs were collected and homogenized. Lung tissue homogenates were serially diluted and titrated on Vero-SLAMF1 cells. Plates were scored microscopically for cytopathic effect (CPE) after 7 days, and the $TCID_{50}$ was calculated.

Please cite this article in press as: Acciani et al., Human neutralizing antibodies targeting the measles virus hemagglutinin and fusion surface proteins, Cell Host & Microbe (2026), https://doi.org/10.1016/j.chom.2026.04.010

mAb/SLAMF1-huFC competition assay

HEK293T cells were transfected with full-length MeV H or F, or mock transfected, for 24 h. Cells were then harvested, washed with PBS, and stained with Cell Proliferation and Encoding V/Blue (Tag-it VioletTM) dye (1:1000 for H+ cells, 1:8000 for F+ cells, and no dye for untransfected cells) (Sartorius #97054) at 37°C for 15 min. Cells were washed twice with cDMEM, resuspended in FACS buffer (2% BSA in PBS), and combined. Cells were then blocked with Human Fc block (1:50, BD #564220), normal goat serum (1:40, Thermo fisher #PCN5000), and normal rat serum (1:40, Stefan Niewiesk) for 15 min at room temperature. Cells were then incubated with each human anti-H mAb (10 μg/mL, this study), human anti-F mAb 3A12 (10 μg/mL, this study), murine anti-H mAb55[37](10 μg/mL), or no mAb, on ice for 30 min. Cells were washed, then incubated with SLAMF1-huFC (100μg/mL) on ice for 30 min. Cells were washed and incubated with rat anti-AviTag-AF647 (1:1000, BioLegend #606760) and goat anti-Human $F(ab')_2$ AF-488 (1:2000, Jackson ImmunoResearch #109-546-097) for 30 min on ice. Cells were washed and resuspended in FACS buffer containing 1X QSol buffer (Sartorius #91304), then analyzed on an iQue3 HTS cytometer (Sartorius).

Measuring H/F thermal stability using nanoDSF

Thermal stabilities of H_{ECT} and F_{ECT} with or without Fab, Fab alone, and buffer-only were measured in triplicate on a NanoTemper Prometheus Panta. Antigen–Fab complexes were incubated at room temperature for 30 min. Data were collected at temperatures ranging from 25°C to 100°C with a 1°C/min temperature ramp and 100% excitation laser power. Unfolding profiles are reported as the first derivative of the intrinsic fluorescence at 330 nm.

mAb Fc effector function analyses

Antibody-dependent cellular phagocytosis (ADCP)

Antibody-dependent cellular phagocytosis was performed as previously described.[97] Briefly, 1 μM neutravidin-labeled yellow-green, fluorescent beads (Thermo Fisher, F8776) were incubated with biotinylated H_{ECT} or F_{ECT}. Beads were spun down and washed twice in 5% BSA in PBS (PBSA) to remove excess unbound antigen, blocked with PBSA for 30 min at RT, and then resuspended at a final dilution of 1:100 in PBS-TBN. Conjugated beads (0.1 μL of the supplied beads or 10 μl of the dilution above) were then incubated for 2 h with a serial dilution of mAb to facilitate Ag-mAb complex formation. Following incubation, 25,000 THP-1 cells/well (ATCC, #TIB-202) were added to complexes in 200 μL THP-1 medium (final volume, RPMI with 10% FBS and 1X Penn-Strep) and incubated for 4 h at 37°C and 5% CO_2. Cells were fixed using 4% PFA and analyzed using flow cytometry (Novocyte-Agilent Technologies). Scores were calculated as the percentage of cells that phagocytosed one or more fluorescent beads multiplied by the mean fluorescent intensity (MFI) of this population. Each antibody was tested in duplicate and values were averaged. The HIV-specific mAb VRC01[98] (1μg/mL) was included as a negative control (not shown). Additional control wells with no added antibody were used to determine the level of antibody-independent phagocytosis.

Reporter cell assay of antibody-dependent cellular cytotoxicity (ADCC)

A surrogate for ADCC activity was measured using a CD16 + (FcγRIIIa) reporter assay system. Jurkat Lucia NFAT (Invivogen, jktl-nfat-cd16) cells were cultured according to the manufacturer's instructions. Cultured cells express CD16, which, when engaged on the cell surface, leads to luciferase expression and secretion. First, high-binding 96-well plates were coated overnight at 4 °C with 1 μg/mL (diluted in ultrapure water) of Neutravidin (Thermo Fisher Cat # 31000). Following incubation, plates were washed with PBST (1XPBS + 0.1% Tween 20) and incubated at room temperature (RT) with 1 μg/mL of biotinylated H_{ECT} or F_{ECT}. After 40 min, plates were washed with PBST twice and blocked with 2.5% BSA in PBS at RT for 1 h. Following plate washing, 100,000 cells per well and a dilution series of each mAb was added to each well in cell culture media lacking selection antibiotics in a 200 μL volume. Following 24 h incubation at 37° C and 5% CO_2, 25 μL of supernatant from each well was transferred into a white optiplate 96-well plate (Fisher Scientific cat# 50-209-9794), and after adding 75 μL of QUANTIluc (Invivogen cat# rep-qlc4lg1) substrate, the plates were read immediately on a SpectraMax luminometer (Molecular Devices) using 1s integration time. Kinetic readings at 0 min, 2.5 min and 5 min were measured, and the mean reading was noted. HIV mAb VRC01 (1μg/ml)[98] was used as an isotype control and the stimulation cocktail (Thermo Fisher Scientific, 00-4970-93) was used as a positive control. Each antibody was tested in duplicate and values were averaged.

Antibody-dependent complement deposition (ADCD)

H mAbs were serially diluted and incubated on a shaker for 2 h at RT with biotinylated antigen-conjugated multiplex assay streptavidin beads prepared as previously described.[99] Guinea pig complement serum (Cedarlane # CL4051) was diluted 1:60 in gelatin veronal buffer (Sigma-Aldrich, GVB++, G6514) and mixed with diluted samples at 37 °C with shaking for 20 min. Following this incubation, cold EDTA solution (15 mM in 1X PBS) was added to prevent further complement activation. After washing, samples were incubated with biotin-conjugated goat anti-C3b (1 μg/mL) (Icllab GC3-60B-Z) at RT for 1 h, followed by staining with Streptavidin-R-Phycoerythrin (Millipore Sigma 42250) reagent per the manufacturer's recommendation. A final wash was performed, and samples were resuspended in sheath fluid and MFI acquired on a FlexMap 3D reader (Luminex). Assay controls included a technical blank (no antibody), heat-inactivated complement serum (not shown), and VRC01. Each antibody was tested in duplicate and values were averaged.

Sample vitrification for Cryo-EM

Cryo-EM grids were prepared with the following sample combinations: H_{ECT}-TS with 1C08 and H_{ECT} with 1C02 were applied to Quantifoil R2/2 copper grids coated with an in-house prepared graphene oxide film, following a previously established protocol.[34] The

H_{ECT}-TS + 1C08 + 4D08 complex was vitrified on C-flat 2/1 grids, while the F_{ECT}2M + 3A12 + 4F09 complex was applied to Quantifoil R2/1 grids, also coated with a graphene oxide layer.

For vitrification, protein complexes were diluted to a final absorbance of 0.1–0.2 at 280 nm. A 3 μL aliquot of each sample was applied to glow-discharged grids using a Vitrobot Mark IV (Thermo Fisher Scientific) operated at 4 °C and ~100% relative humidity. After a 15-s incubation, grids were blotted for 1.5–3 s using blot force setting 0 and a drain time of 0.5 s. The grids were immediately plunge-frozen in liquid ethane, cooled by liquid nitrogen, and stored under cryogenic conditions until imaging.

Data acquisition, processing, and model building

Cryo-EM data were collected on a FEI Titan Krios transmission electron microscope operated at a nominal magnification of 130,000×, and equipped with a Gatan K3 direct electron detector and a 20 eV energy filter. The calibrated physical pixel size was 0.66 Å/pixel. All datasets were processed using cryoSPARC v4.6.2 (Structura Biotechnology Inc.). Initial particle picking was performed in live sessions using the blob picker in over-picking mode (particle diameter range: 80–120 Å; minimum distance: 0.5×diameter). Approximately 5 million particles were initially extracted per dataset and Fourier-binned to 64 pixels to accelerate fast classification steps. Particles corresponding to the target complex were identified using Deep2D classification.[34]

Subsequent rounds of non-uniform and heterogeneous refinement were performed to isolate high-quality particles, from which ~10,000 particles were selected for training a Topaz particle picker (10 training epochs). Particles picked by Topaz were also binned to 64 pixels and subjected to iterative refinement and classification. High-quality particles were then re-extracted at 160 pixels for improved alignment, achieving a resolution limit of ~5 Å, which enabled further discrimination of conformational heterogeneity via 3D classification.

A final round of particle re-extraction was performed with binning adjusted to produce a Fourier shell correlation (FSC) of 0.143 at approximately 75% of Nyquist resolution, corresponding to Fourier-cropped particle box sizes of 320–360 pixels. Final refinements used non-uniform refinement with symmetry: C2 for H_{ECT} complexes and C3 for F_{ECT}2M. For H_{ECT} datasets, symmetry expansion (C2) was followed by 3D classification and local refinement.

Initial structural models were generated using AlphaFold2 and AlphaFold3 predictions for the H_{ECT} and Fab fragments. The cryo-EM structure of F_{ECT}-2M (PDB ID: 8UUP) was used as a starting model. All initial models were rigid-body fitted into the density maps and further refined using ISOLDE. Manual adjustments were performed in Coot, and final real-space refinement was performed in Phenix v2.0-rc.

Structural analysis

Antibody–protein interfaces were analyzed using the Protein Interfaces, Surfaces and Assemblies (PISA) tool within the CCP4 suite. Local root-mean-square deviation (RMSD) analyses were performed using a custom Python script. In this approach, structurally aligned chains from two models were superimposed using the Superimposer module from Biopython, and residue-resolved deviations were calculated based on Cα–Cα distances derived from the sequence alignment. This technique allowed quantification of localized conformational differences across distinct structural states.

The most representative H ectodomain structure was identified through complete pairwise structural comparisons and global RMSD calculations. The structure exhibiting the lowest average RMSD relative to all others was selected as the reference, corresponding to PDB ID: 2RKC.

To model the β-sheet register shift, a full-length H ectodomain model was generated using AlphaFold3. This model was then compared to the reference structure (2RKC) and compared to the determined cryo-EM structures of H in complex with antibodies or previously described X-ray structures.

Sequence conservation analysis

Sequence conservation analysis for both H and F glycoproteins was performed using curated datasets obtained via the SPACE (https://github.com/dzyla/SPACE). Sequences were filtered against the respective reference entries from UniProt (H: Q786F2; F: Q786F3) and aligned using FAMSA (Fast and Accurate Multiple Sequence Alignment), a tool optimized for large datasets. H and F sequences in the dataset include naturally occurring and lab-adapted MeV strains.

Per-residue conservation scores were computed using the AL2CO program.[86] First, amino acid frequencies at each position were estimated using the ''estimated independent counts method,'' and a conservation index was calculated using the frequencies and the ''entropy-based measure strategy'' formula:

$$C^e(i) = \sum_{a=1}^{20} f_a(i) \times ln\, f_a(i).$$

$C^e(i)$: entropy-based conservation score at position i

$f_a(i)$: frequency of amino acid a at position i in the multiple sequence alignment

Conservation indices were normalized using the mean conservation across positions and the standard deviation of conservation scores, generating Z-scores. Z-scores were mapped onto the corresponding PDB structures via the B-factor column for structural visualization. Fully conserved residues were indexed at 1.482 for H_{ECT} and 0.829 for F_{ECT}, owing to differences in the number of sequences available for each protein.

Please cite this article in press as: Acciani et al., Human neutralizing antibodies targeting the measles virus hemagglutinin and fusion surface proteins, Cell Host & Microbe (2026), https://doi.org/10.1016/j.chom.2026.04.010

QUANTIFICATION AND STATISTICAL ANALYSES

All statistical analyses were performed using Graphpad Prism 10.

Sequence analyses

CDRH3 lengths, VH residue mutation counts, affinities, and % MeV infection were tested for normality. Correlations were examined by determining the Spearman nonparametric correlation coefficients (r) and P-values for each comparison.

In vitro neutralization of rMeV-B3-mCherry

MCherry-infected cells were counted using a CellInsight CX5 plate reader (ThermoFisher). The samples were tested in three to four experiments. The measurements from each plate were normalized using mAb^-/MeV^+ wells. Data were analyzed in GraphPad Prism 10 and are shown as normalized percent MeV inhibition (Figure 4A). We used the nonlinear regression agonist vs normalized response (variable slope) model to determine half-maximal inhibitory concentrations (IC_{50}s) for each mAb.

In vitro viral neutralization of MeV genotypes B3, D8, and the Schwartz vaccine strain

Infected fluorescent cells were counted using a Cytation 5 (BioTek) and analyzed with Gen5 3.11 software (min object size 25 μm, max object size 135 μm, threshold 3,000). The samples were tested in three independent experiments. The measurements from each plate were normalized using mAb^-/MeV^+ wells. Data were analyzed in GraphPad Prism 10 and are shown as normalized percent MeV inhibition (Figure 5C). We used the nonlinear regression agonist vs normalized response (variable slope) model to determine IC_{50}s for each mAb.

In vivo mAb prophylactic and therapeutic protection in cotton rats

We analyzed both raw and normalized lung tissue viral titers using one-way ANOVAs (not assuming equal standard deviations) to compare mAb vs control (PBS) lung titer reductions (log10/g lung tissue), with the Dunnett's multiple comparisons correction. Because lung titers for animals prophylactically treated with mAb 4F09 all fell below the 10^2 $TCID_{50}$/g lung tissue threshold of detection, the nonparametric Mann-Whitney test was used. Average raw titers for prophylactic treatments are shown in Figure S5A grouped in the chronological order animals were assessed. For the normalized data in Figures 4B and 7B, we subtracted average PBS-treated lung titers ($TCID_{50}$log10/g lung tissue) from mAb-treated lung titers ($TCID_{50}$log10/g lung tissue) and show the average reduction of lung titers ($TCID_{50}$log10/g lung tissue) for each mAb treatment. We compared therapeutic mAb treatments to each other and PBS controls within the +24h and +48h groups using a one-way ANOVA multiple comparisons test with Tukey's correction. Normalized prophylactic and therapeutic treatment regimens were compared for each mAb by two-way ANOVA multiple comparisons test with Tukey's correction. * $p<0.05$, ** $p<0.005$, *** $p<0.0005$, *** $p<0.0001$.

mAb/SLAMF1-huFC competition assay

Cells stained for mAb and receptor binding were analyzed on an iQue3 HTS cytometer (Sartorius). Live, single cells were gated using forward and side scatter, and H+, F+, and untransfected cells were gated using encoder dye fluorescence. The percentage of cells positive for mAb-binding fluorescence (AF488) and SLAMF1-binding fluorescence (AF647) were quantified. Background values from secondary-only (no mAb or SLAMF1-huFC) controls were subtracted. Proportions of mAB+ and SLAMF1+ cells were averaged across three independent experiments. Statistical analyses of SLAMF1-binding across H+, F+, and untransfected cells was performed using a 2-way ANOVA with Tukey's multiple comparisons correction to compare the numbers of SLAMF1+ cells with mAb versus SLAMF1+ cells with no mAb added; **** $p<0.0001$.